DRAFT VERSION OCTOBER 4, 2016
Preprint typeset using LaTeX style AASTeX6 v. 1.0

THE INFLUENCE OF MAGNETIC FIELDS ON ABSORPTION AND EMISSION SPECTROSCOPY

HESHOU ZHANG[1,2] , HUIRONG YAN[1,2] & PHILIPP RICHTER[2,3]

[1]Deutsches Elektronen-Synchrotron DESY, Platanenallee 6, D-15738 Zeuthen, Germany;

[2]Institut fr Physik und Astronomie, Universitt Potsdam, Haus 28, Karl-Liebknecht-Str. 24/25, D-14476 Potsdam, Germany;

[3]Leibniz-Institut fr Astrophysik Potsdam(AIP), An der Sternwarte 16, D-14482 Potsdam, Germany;

ABSTRACT

Spectroscopic observations play essential roles in astrophysics. They are crucial for determining important physical parameters, providing information about the composition of various objects in the universe, as well as depicting motions in the universe. However, spectroscopic studies often do not consider the influence of magnetic fields. In this paper, we explore the influence of magnetic fields on the spectroscopic observations arising from Ground State Alignment (GSA). Synthetic spectra are generated to show the measurable changes of the spectra due to GSA. The influences of atomic alignment on absorption from DLAs, emission from H II Regions, submillimeter fine-structure lines from star forming regions are presented as examples to illustrate the effect in diffuse gas. Furthermore, we demonstrate the influence of atomic alignment on physical parameters derived from spectral line ratios, such as the alpha-to-iron ratio([X/Fe]), interstellar temperature, and ionization rate. Results in our paper show that due to GSA, magnetic fields will affect the spectra of diffuse gas with high signal-to-noise(S/N) ratio under the condition that photon-excitation is much more efficient than thermal collision.

Keywords: HII regions–ISM: abundances–ISM: lines and bands–magnetic fields–methods: observational–submillimeter: ISM

1. INTRODUCTION

Spectroscopy plays a crucial role in studying the universe. Absorption spectroscopy proves to be an important tool for the analysis of chemical abundances (e.g., Fox et al. 2013; Richter et al. 2013; Welsh & Lallement 2012a; Miller & Bregman 2015), interstellar environment detection (e.g. Howk et al. 2005) and chemical evolution of circumburst medium of GRB (e.g., Fynbo et al. 2006); emission spectra help the modeling of stellar atmosphere (e.g., Pickering et al. 2001), supernova explosion (e.g., Jerkstrand et al. 2011) and the study of narrow line emission from active galactic nuclei (e.g., Bruhweiler & Verner 2008); FIR submillimeter fine structure lines provide abundant information in star forming regions (e.g., Stutzki et al. 1988; Ceccarelli et al. 1996), etc. However, astrophysical magnetic fields, which exist everywhere in the universe, are not often considered in spectroscopic studies. As demonstrated in Yan & Lazarian (2006, 2007, 2008), magnetic fields redistribute the angular momenta of atoms of diffuse medium among different sublevels on the ground state (known as Ground State Alignment, hereby GSA), and hence, influence the polarization of scattering and absorption from the medium. In this paper, we will study the influence of magnetic fields through GSA effect on astrophysical spectroscopy.

GSA is a universal phenomenon in any diffuse medium where the radiation anisotropy is present. Alignment refers to the orientation of the angular momentum of atoms. Occupations of the atoms on different sublevels of the ground state will alter when there exists anisotropic radiation field. With the existence of magnetic fields, the angular momenta of the atoms will redistribute among the sublevels on the ground state due to fast magnetic precession, which is termed as magnetic realignment (see Yan & Lazarian 2012, 2013 for details). GSA has been a well-developed theory. Optical pumping was firstly proposed by Kastler (1950), and then the atomic alignment in the presence of magnetic fields was studied in laboratory (see Hawkins 1955). Toy models of this effect were proposed by Varshalovich (1968, 1971). Then, emission for atoms with idealized fine structure given a particular geometry of magnetic fields and light beam was discussed in Landolfi & Landi Degl'Innocenti (1986).

Calculations for GSA with fine and hyperfine structure in astrophysical environment were provided in Yan & Lazarian (2006, 2007, 2008). They revealed GSA as a unique tracer for 3D magnetic fields in diffuse medium. Zhang et al. (2015) demonstrated the existence of GSA in general radiation fields with anisotropy.

Owing to GSA, magnetic fields will have a notable influence on spectra observed. As illustrated in Yan & Lazarian (2012), GSA is effective when ν_L (Larmor precession rate) $> \tau_R^{-1}$ (radiative pumping rate) $> \tau_c^{-1}$ (collisional transition rate), which means

a broad range of applicabilities of GSA in any diffuse medium with magnetic fields up to 1 Gauss and approximately down to the scale smaller than micro Gauss where the diffuse medium is quite close[1] to the pumping source. Even longer distance from the pumping source to the diffuse medium allows even smaller magnetic fields to align the medium (down to 10^{-15} Gauss, see Yan & Lazarian 2012)[2]. Since the mean magnetic field in the galaxy spiral arm is of the order of 1 10μG, spectra observed from the diffuse medium in the galaxy, e.g. DLAs, are no doubt affected by GSA. As long as the strength of magnetic field is within the applicable range of GSA, the main influence of the magnetic fields on the spectrum is due to the change of atomic angular momentum distribution arising from GSA.

In this paper, the basic physical parameters of GSA are defined in §2. In §3, we use several examples of diffuse gas in different astrophysical environment to illustrate the influence of GSA effect on different types of spectra. Synthetic spectra for absorption lines are generated according to a scenario of DLAs in galaxy. The influence of GSA on different emission lines are compared according to a scenario of extragalactic H II Regions. Results on submillimeter fine-structure lines are presented in Star Forming Regions. In §4, the influences of GSA on different astrophysical properties derived from spectral line ratios are demonstrated in different subsections. Discussions and conclusions are presented in §5 and §6.

2. PRINCIPLE PHYSICAL PARAMETERS

The theory of GSA has been comprehensively illustrated in Yan & Lazarian (2006, 2007, 2008). Thus we present below briefly the main physical parameters used to depict the alignment and its influence on spectra. For detailed definition of the physical parameters and formulae, readers may refer to Appendix A.

The absorption from the state where the atoms are aligned is polarized, due to a difference of absorption parallel and perpendicular to the direction of alignment. Stokes parameters for absorption lines with finite optical depth are:

$$\begin{aligned} I &= (I_0+Q_0)e^{-\tau(1+\frac{\eta_1}{\eta_0})}+(I_0-Q_0)e^{-\tau(1-\frac{\eta_1}{\eta_0})},\\ Q &= (I_0+Q_0)e^{-\tau(1+\frac{\eta_1}{\eta_0})}-(I_0-Q_0)e^{-\tau(1-\frac{\eta_1}{\eta_0})},\\ U &= U_0e^{-\tau}, V = V_0e^{-\tau}, \end{aligned} \tag{1}$$

in which I_0, Q_0, U_0, V_0 are the Stokes parameters of the background radiation. $\eta_i(i=0\sim 3)$ are the corresponding absorption coefficients, which are defined as (Landi Degl'Innocenti 1984, see also Yan & Lazarian 2006):

$$\eta_i(\nu,\Omega) = \frac{h\nu_0}{4\pi}Bn(J_l)\Psi(\nu-\nu_0)\sum_{KQ}(-1)^K\omega^K_{J_lJ_u}\sigma^K_Q(J_l)\mathcal{J}^K_Q(i,\Omega), \tag{2}$$

where the quantity $\sigma^K_Q\equiv\frac{\rho^K_Q}{\rho^0_0}$ is the alignment parameter, the quantity ρ^K_Q is the density matrix[3] that can be influenced by magnetic fields due to GSA (this point is further discussed in Appendix A). The quantity $\omega^k_{J_lJ_u}\equiv\left\{\begin{array}{ccc}1&1&K\\J_l&J_l&J_u\end{array}\right\}/\left\{\begin{array}{ccc}1&1&0\\J_l&J_l&J_u\end{array}\right\}$. As illustrated in (Yan & Lazarian 2006), the alignment parameter is related to θ_{br}, the angle between the direction of radiation and magnetic direction[4]. The quantity B is Einstein coefficient for absorption[5]. The total atomic population $n(J_l)$ on the lower level J_l is defined as $n\sqrt{[J_L]}\rho^0_0(J_l)$. $\Psi(\nu_-\nu_0)$ is the line profile. The quantity $\mathcal{J}^K_Q(i,\Omega)$ is the irreducible radiation tensor of incoming light averaged over the whole solid angle and the line profile:

$$\begin{aligned} \mathcal{J}^0_0(i,\Omega) &= \begin{pmatrix}1\\0\\0\end{pmatrix}, \mathcal{J}^2_0(i,\Omega) = \frac{1}{\sqrt{2}}\begin{bmatrix}1-1.5\sin^2\theta\\-3/2\sin^2\theta\\0\end{bmatrix},\\ \mathcal{J}^2_{\pm2}(i,\Omega) &= \sqrt{3}e^{\pm2i\phi}\begin{bmatrix}\sin^2\theta/4\\-(1+\cos^2\theta)/4\\\mp i\cos\theta/2\end{bmatrix}, \mathcal{J}^2_{\pm1}(i,\Omega) = \sqrt{3}e^{\pm i\phi}\begin{pmatrix}\mp\sin2\theta/4\\\mp\sin2\theta/4\\-i\sin\theta/2\end{pmatrix}. \end{aligned} \tag{3}$$

the quantity $\mathcal{J}^K_Q(i,\Omega)$ is decided by its direction $\Omega(\theta,\phi)$, where θ is defined as the angle between the line of sight and the

[1] the distance on the scale of several Au

[2] It is only a rough estimate here. Specific limits depend not only the distance and type of radiation source, but also the collisions determined by gas density.

[3] For example, the irreducible tensor for $J/F=1$ is $\rho^2_0=[\rho(1,1)-2\rho(1,0)+\rho(1,-1)]$.

[4] Note that all the angles used in the paper are listed in Appendix C.

[5] The data of Einstein coefficients used in the paper are taken from the Atomic Line List (http://www.pa.uky.edu/~peter/atomic/) and the NIST Atomic Spectra Database.

magnetic direction. In the optical thin case, where τ is proportional to the column density of the absorbing species, the change in the absorption coefficients from the GSA is proportional to the absorption depth of the line.

Moreover, the influence of magnetic fields on upper level is negligible when the magnetic precession rate is larger than the emission rate of upper level. The differential occupation the on ground state which results from the atomic alignment is transferred to the upper atomic states by radiative excitation (see Yan & Lazarian 2012 for details). The emission coefficients ε_i demonstrating the polarized emission from the upper level are (see Yan & Lazarian 2007):

$$\varepsilon_i(\nu,\Omega) = \frac{h\nu_0}{4\pi} An(J_u,\theta_{br})\Psi(\nu-\nu_0)\sum_{KQ}\omega^K_{J_uJ_l}\sigma^K_Q(J_u,\theta_{br})\mathcal{J}^K_Q(i,\Omega). \quad (4)$$

where the intensity of emission line is when $i = 0$. The quantity A is Einstein coefficient for emission.

Throughout the paper, we set the case when the magnetic field is parallel to the incidental radiation as 1 and use the ratio between the cases with the change of the direction of magnetic field and this case to demonstrate the variation of spectra with the influence of magnetic field due to GSA. When the magnetic field is parallel to the incident radiation, only the anisotropy of the radiation field contribute to the alignment, thus we can consider that there is no magnetic realignment in this case. Moreover, for the sake of observation, the change of magnetic fields is presented in the observational coordinate system (θ,ϕ). The reason for the choice of the coordinate system is discussed in Appendix B.

In the following, we will evaluate more quantitatively the influence of magnetic fields on absorption and emission spectral lines due to GSA. We will also discuss under what conditions a direct measurement of the GSA effect is possible with current observational data.

3. INFLUENCE OF GSA ON SPECTRA

3.1. *Influence of GSA on absorption spectra*

3.1.1. *Typical scenario for absorption spectra*

As an example, we show in Fig.1 a typical scenario, in which the effect of atomic alignment could lead to measurable effect in observational data. Given is a typical late-type galaxy with an extended neutral gas disk and an interstellar magnetic field. Star-formation is expected to take place in distinct regions in the disk (i.e., in spiral arms), so that at a given point in the disk the interstellar radiation field might be highly anisotropic. Imagine a bright background point source (e.g., a QSO) being located behind the gas disk. In the spectrum of the background QSO, the gas disk will leave its imprint through many absorption lines from neutral and ionized species, where most of the lines are located in the (restframe) UV. Such disk absorbers are known to contribute to the population of the so-called Damped Lyman α absorbers (DLAs) that are frequently observed at low and high redshift in QSO spectra. If in the region in which the sightlines pierces the disk the geometry of the ambient magnetic field and the anisotropy of the interstellar radiation field is fortunate, the atomic alignment will cause small but measurable changes in the central absorption depths of unsaturated absorption lines. Due to a small density in the interstellar medium, the collision rate is much smaller than the Larmor precession rate. Hence, the magnetic realignment is effective. Latter part of this section will illustrate the variation of line intensity with the influence of magnetic fields.

3.1.2. *Influence on absorption lines*

The alignment of singly-ionized sulfur S II absorption line in a beam of light is demonstrated in Yan & Lazarian (2006). The ground state of S II is $4S^o_{\frac{3}{2}}$ ($J_l = \frac{3}{2}$) and the upper states are $4P_{\frac{1}{2},\frac{3}{2},\frac{5}{2}}$ ($J_u = \frac{1}{2},\frac{3}{2},\frac{5}{2}$). The transition wavelength from ground the level to three upper levels are 1250.58, 1253.81, 1259.52 Å, respectively.

The three transitions of singly-ionized sulfur (S II; upper ionization potential 23.3 eV) at $\lambda\lambda 1250.58, 1253.81, 1259.52$ represent important tracers for neutral and weakly ionized gas in the local interstellar and circumgalactic medium and in gas in distant galaxies (e.g., Kisielius et al. 2014; Welsh & Lallement 2012b; Richter et al. 2001; Fox et al. 2014a). Sulfur is an α element, but shows only a weak depletion into dust grains (e.g.,Savage & Sembach 1996), so that the interstellar S abundance is often used as a proxy for the α-abundance in the gas. The three lines mentioned above span a moderate oscillator strengths (Kisielius et al. 2014; Morton 2003) are all within 10 Å, so that in an UV or optical (if absorption is red-shifted) spectrum, these lines can be observed in the same wavelength region at an identical S/N. In addition, sulfur has a relatively low cosmic abundance (Asplund et al. 2009), so that under typical interstellar conditions (in particular in low-metallicity environments) these lines are not saturated. Thus, the S II $\lambda\lambda 1250.58, 1253.81, 1259.52$ represent the ideal transitions to study atomic alignment effects in interstellar environments with magnetic fields. Let's denote the real intensity of absorption line as I^{ab}_{re}, which is proportional to real column density τ_0; and the observed intensity of absorption lines as I^{ab}_{ob}, which is proportional to the varied column density $\tau_0 \pm \Delta\tau$. The ratio between observed absorption line intensity and real line intensity is defined by

$$r^{ab}(\lambda,\theta_0,\theta_{br},\theta) = I^{ab}_{ob}/I^{ab}_{re} \propto \left(\rho^0_0(J_l)\sqrt{2} + \omega^2_{J_lJ_u}\rho^2_0(J_l)\left(1-1.5\sin^2\theta\right)\right), \quad (5)$$

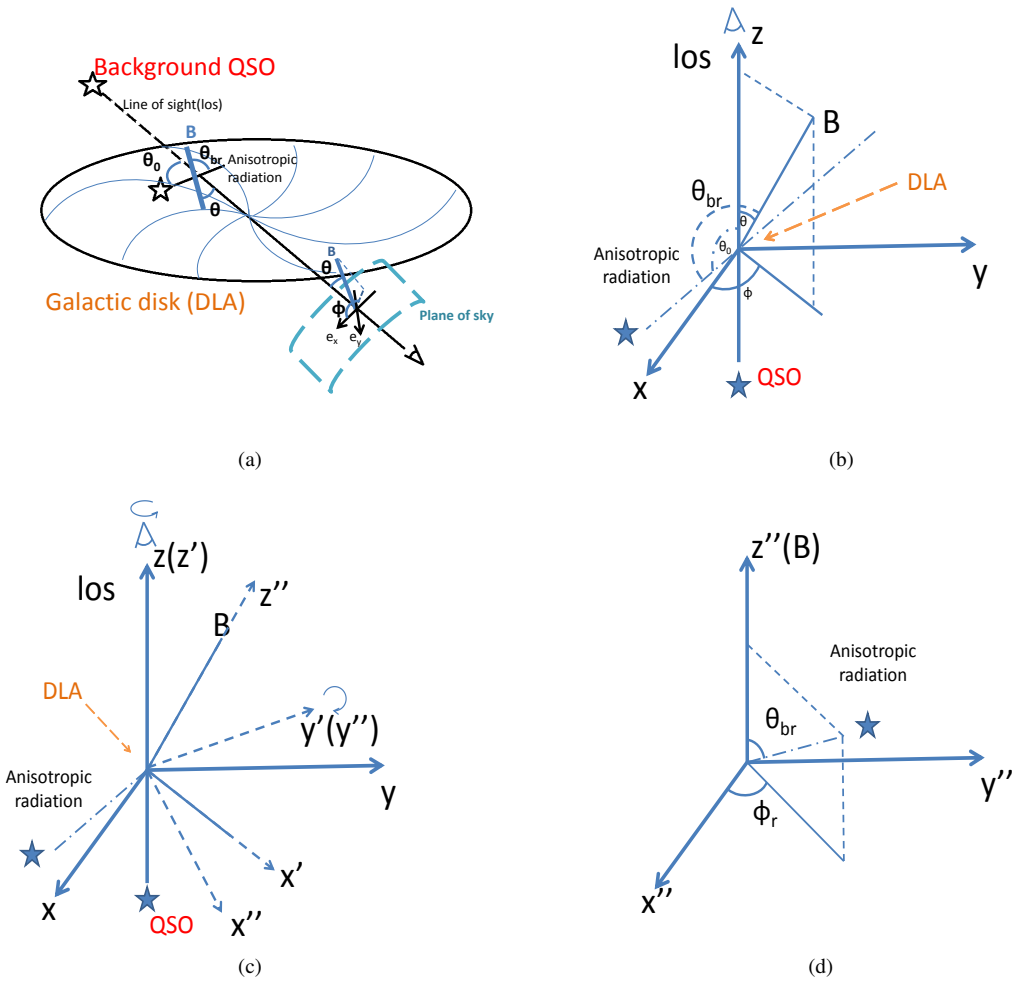

Figure 1. Scenario for atomic alignment in interstellar medium in galaxy. (a) Typical environment where absorption line is polarized owing to GSA. Alignment is produced by a pumping source, which both influence the polarization of scattering(emission) lines and induce polarization on absorption of another background source from which the light passes through the aligned medium[6]. θ_{br}, θ are the polar angles of the pumping radiation and line of sight measured in reference to the magnetic field, respectively. θ_0 is the angle between the anisotropic radiation and the line of sight; (b) $xyz-$coordinate system with the line of sight being $z-$axis, which is the main coordinate system to compare the change of magnetic fields (see more details in Appendix A); (c) Coordinate system transformation: first rotate line of sight and make the magnetic field on $x'z'-$plane to form $x'y'z'-$coordinate system, and then rotate $y'-$axis to make $x''y''z''-$coordinate system with the magnetic field being z''-axis; (d) $x''y''z''-$coordinate system with the magnetic field being z''-axis.

where λ is the wavelength of the line, $\theta_0, \theta_{br}, \theta$ are defined in Fig. 1(a). The optical depth variations with respect to different magnetic field direction are presented in Fig. 2 given line of sight perpendicular to radiation direction($\theta_0 = 90°$), radiation source temperature $T_{source} = 50000K$. By comparing Fig. 2(a), Fig. 2(b), and Fig. 2(c), it is obvious that with the same direction of radiation and line of sight, the influence of magnetic fields on different spectral lines is different.

Moreover, even for the same spectrum with the same radiation field observed from the same line of sight (hereby, the same θ_0), the actual column density deduced from the spectrum can be different only due to the change of magnetic fields. For example, as demonstrated in Fig. 2(a), the magnetic field does not influence the spectrum when the direction of the magnetic field is parallel to the line of sight ($\theta = 0°$), whereas enrich 7% of the spectrum when the direction of the magnetic field is perpendicular to both the line of sight and incident radiation ($\theta = 90°, \phi = 90°$). Therefore, magnetic fields can affect the column density deduced from the absorption line observed due to GSA.

In Fig.3 we show the expected maximum effect of the atomic alignment for the three S II lines in an synthetic absorption spectrum of a DLA for $\theta_0 = 90°$. To show the effect clearly, we zoom in the spectrum to the radial velocity range

[6] There could be degenerate case where the pumping source is the same as the background source (see Yan & Lazarian 2006).

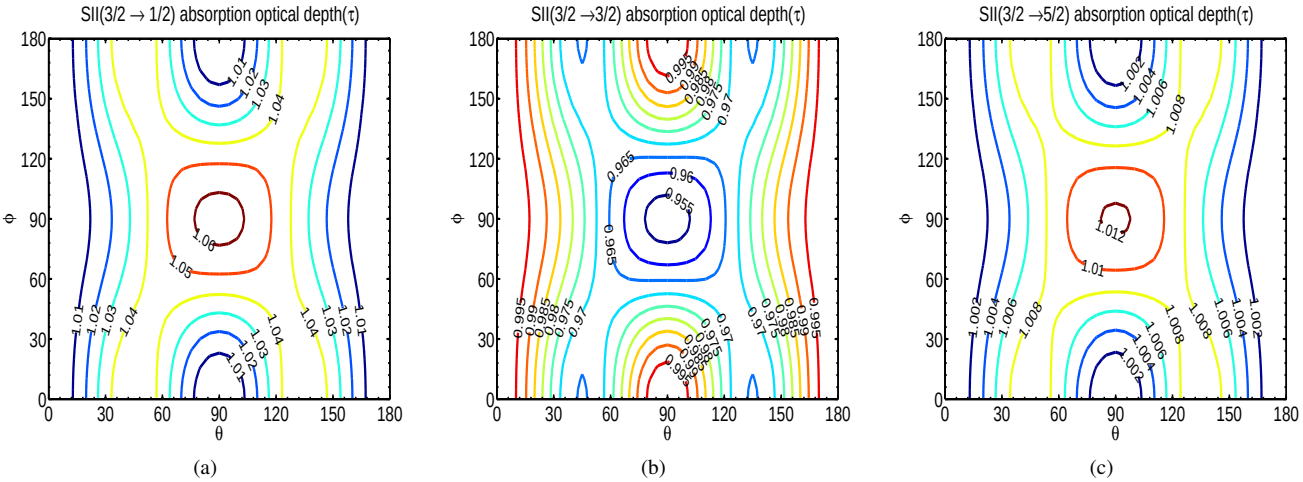

Figure 2. S II absorption line in blackbody radiation with $T_{source} = 50000K$. The variation of line intensity with respect to the direction of the magnetic field is compared between the line (a)1250.58Å, (b)1253.81Å and (c)1259.52Å in the case of line of sight vertical to radiation field($\theta_0 = 90^\circ$). θ and ϕ are the polar and azimuth angle of the magnetic field in line of sight coordinate defined in Fig. 1(b).

$[-10km{\cdot}s^{-1}, 10km{\cdot}s^{-1}]$. It is obvious that the alignment enriches λ1250.58 whereas depletes λ1253.81, and λ1259.52 in different scales. Hence, magnetic fields have a small yet measurable effect on the spectra observed and should be taken into consideration for the error budget of spectroscopic studies.

Fig. 4(a) and Fig. 4(b) provide an overview on the maximum and minimum column density variations from different absorption lines with (a) $\theta_0 = 45^o$ and (b) $\theta_0 = 90^o$, respectively. The more comprehensive results for maximum and minimum variations of column density for different absorption lines are presented in Table 1[7], where $\Delta N/N_{max}$ means enrichment and $\Delta N/N_{min}$ means depletion. Since chemical abundance studies always compare the log-scale of column density, the variations due to GSA on log-scale are also presented. For $\theta_0 = 90^o$, S II λ1250.58 can be enriched to the maximum of 7% whereas S IV λ1072.97 can be depleted to the maximum of 27%; S I λ1474.57 can be depleted to the maximum of 22% whereas the same line can be enriched to the maximum of 2% (see Fig. 4(b)). Therefore, magnetic fields have different influences on different spectral lines, as well as on the same spectral line with different direction of magnetic field.

3.2. *Magnetic influence on emission spectra*

Emission spectra are very important in astrophysical studies. UV emission lines are used to model stellar wind (Leitherer et al. 2016). Optical recombination emission lines can help the analysis of chemical abundance in H II regions and Planetary Nebulae (PNe) (e.g., García-Rojas et al. 2016; Peimbert & Peimbert 2006), and they have the advantages that they are not severely affected by the uncertainty of reddening correction as collision excited lines and they can directly analyze the ionized gas phase chemical (e.g., Esteban et al. 2014). Combined with absorption spectra, emission spectra can provide even more information, e.g., gas condition in DLAs (e.g., Meiring et al. 2011; Kisielius et al. 2014).

3.2.1. *Scenario for emission spectra*

As an example, we show in Fig.5 a typical scenario, where GSA affects the observational emission data. Presented is a typical spiral galaxy with diffuse emission nebulae (H II regions, which mostly reside on the spiral arms of the galaxies) denoted in red circle and interstellar magnetic fields on the disk. Stars in the H II region ionise and illuminate the surrounding medium, from which the emission lines can be observed. Radiation field here[8] is expected to have a certain degree of anisotropy. With the influence of magnetic fields and anisotropic radiation field, the ground state of the atoms in diffuse gas will be aligned and the alignment will be transferred to upper states due to optical excitation, which results in polarized spontaneous emission. This scattering process due to GSA will cause measurable changes in the emission spectra observed. Small density of the diffuse medium in H II region promises a much smaller collision rate than Larmor precession rate, which makes atomic alignment effective. Latter part of this section will present the variation of the emission spectra with the influence of GSA.

[7] We present not only the absorption from the ground state, but also from some sublevels that have small energy difference with the ground state. Some of these lines can be detected at the places like galactic halos (Richter et al. 2013; Fox et al. 2014b) and circumburst medium in GRB(Fynbo et al. 2006). For example, according to Boltzmann distribution, when the medium temperature reaches the scale of a couple of hundred K, the metastable state C II*($J = 3/2$) will resides the same scale of atoms as the ground state C II($J = 1/2$) (see §2 in Yan & Lazarian 2012 for details).

[8] As illustrated in Zhang et al. (2015), alignment also exists in extended radiation source like cluster of stars. For simplicity, the radiation source considered here has been treated as a single pumping star.

Table 1. COLUMN DENSITY VARIATIONS FOR ABSORPTION LINE INDUCED BY GSA

Species	Transition	Wavelength	$\Delta N/N_{min}$	$\Delta N/N_{max}$	$\Delta \log(N/N_0)_{min}$	$\Delta \log(N/N_0)_{max}$
O I	$3P_2 \rightarrow 3D^\circ$	1025.76Å	-6.37%	$+0\%$	-2.86×10^{-2}	0
S I	$3P_2 \rightarrow 3D^\circ_1$	1474.57Å	-27.29%	$+1.81\%$	-1.38×10^{-1}	7.79×10^{-3}
	$3P_2 \rightarrow 3D^\circ_2$	1474.38Å	-22.82%	$+2.62\%$	-1.13×10^{-1}	1.12×10^{-2}
	$3P_2 \rightarrow 3D^\circ_3$	1473.99Å	-19.99%	$+0.08\%$	9.69×10^{-2}	3.65×10^{-4}
S II	$4S^\circ_{\frac{3}{2}} \rightarrow 4P_{\frac{1}{2}}$	1250.58Å	-7.56%	$+6.33\%$	-3.41×10^{-2}	2.67×10^{-2}
	$4S^\circ_{\frac{3}{2}} \rightarrow 4P_{\frac{3}{2}}$	1253.81Å	-4.71%	$+7.00\%$	-2.09×10^{-2}	2.94×10^{-2}
	$4S^\circ_{\frac{3}{2}} \rightarrow 4P_{\frac{5}{2}}$	1259.52Å	-1.61%	$+1.22\%$	-7.04×10^{-3}	5.29×10^{-3}
Ti II	$a4F_{\frac{3}{2}} \rightarrow z4D^\circ_{\frac{1}{2}}$	3072.97Å	-1.64%	$+1.30\%$	-7.16×10^{-3}	5.62×10^{-3}
	$a4F_{\frac{3}{2}} \rightarrow z4F^\circ_{\frac{3}{2}}$	3241.98Å	-1.03%	$+1.35\%$	-4.48×10^{-3}	5.81×10^{-3}
	$a4F_{\frac{3}{2}} \rightarrow z4F^\circ_{\frac{5}{2}}$	3229.19Å	-0.33%	$+0.26\%$	-1.44×10^{-3}	1.12×10^{-3}
Fe II	$a6D_{\frac{9}{2}} \rightarrow y6F^\circ_{\frac{7}{2}}$	1142.36Å	-1.69%	$+4.42\%$	-7.40×10^{-3}	1.88×10^{-2}
	$a6D_{\frac{9}{2}} \rightarrow y6F^\circ_{\frac{9}{2}}$	1143.22Å	-2.86%	$+7.94\%$	-1.26×10^{-2}	3.32×10^{-2}
	$a6D_{\frac{9}{2}} \rightarrow y6F^\circ_{\frac{11}{2}}$	1144.93Å	-0.46%	$+3.21\%$	-2.02×10^{-3}	1.37×10^{-2}
Absorption from other sublevels of the ground level						
C I*	$3P_1 \rightarrow 3P^\circ_0$	1260.93Å	-24.20%	$+1.54\%$	-1.20×10^{-1}	6.64×10^{-3}
	$3P_1 \rightarrow 3P^\circ_1$	1261.00Å	-17.45%	$+0.46\%$	-8.33×10^{-2}	2×10^{-3}
	$3P_1 \rightarrow 3P^\circ_2$	1261.12Å	-15.76%	$+0\%$	-7.45×10^{-2}	0
C II*	$2P^\circ_{\frac{3}{2}} \rightarrow 2S_{\frac{1}{2}}$	1037.02Å	-9.02%	$+3.68\%$	-4.10×10^{-2}	1.57×10^{-2}
	$2P^\circ_{\frac{3}{2}} \rightarrow 2D_{\frac{3}{2}}$	1335.66Å	-10.34%	$+1.29\%$	-4.74×10^{-2}	5.56×10^{-3}
	$2P^\circ_{\frac{3}{2}} \rightarrow 2D_{\frac{5}{2}}$	1335.71Å	-5.39%	$+0.10\%$	2.41×10^{-2}	4.41×10^{-4}
O I*	$3P_1 \rightarrow 3D^\circ$	1027.43Å	-9.57%	$+0\%$	-4.37×10^{-2}	0
Si II*	$2P^\circ_{\frac{3}{2}} \rightarrow 2D_{\frac{3}{2}}$	1264.74Å	-5.59%	$+5.32\%$	2.50×10^{-2}	2.25×10^{-2}
	$2P^\circ_{\frac{3}{2}} \rightarrow 2D_{\frac{5}{2}}$	1265.00Å	-3.00%	$+0.27\%$	-1.32×10^{-2}	1.18×10^{-3}
S I*	$3P_1 \rightarrow 3P^\circ_0$	1303.11Å	-21.05%	$+1.72\%$	-1.03×10^{-1}	7.41×10^{-3}
	$3P_1 \rightarrow 3P^\circ_1$	1302.86Å	-14.43%	$+0.50\%$	-6.77×10^{-2}	2.18×10^{-3}
	$3P_1 \rightarrow 3P^\circ_2$	1302.34Å	-12.74%	$+0\%$	-5.92×10^{-2}	0
S III*	$3P_1 \rightarrow 3P^\circ_0$	1015.50Å	-24.67%	$+1.53\%$	-1.23×10^{-1}	6.58×10^{-3}
	$3P_1 \rightarrow 3P^\circ_1$	1015.57Å	-17.88%	$+0.46\%$	-8.56×10^{-2}	1.99×10^{-3}
	$3P_1 \rightarrow 3P^\circ_2$	1015.78Å	-16.19%	$+0\%$	-7.67×10^{-2}	0
S IV*	$2P^\circ_{\frac{3}{2}} \rightarrow 2D_{\frac{3}{2}}$	1072.97Å	-1.20%	$+2.20\%$	-5.25×10^{-3}	9.46×10^{-3}
	$2P^\circ_{\frac{3}{2}} \rightarrow 2D_{\frac{5}{2}}$	1073.52Å	-0.20%	$+0.56\%$	-8.68×10^{-4}	2.43×10^{-3}
C I**	$3P_2 \rightarrow 3D^\circ_1$	1193.65Å	-24.65%	$+1.06\%$	-1.23×10^{-1}	4.60×10^{-3}
	$3P_2 \rightarrow 3D^\circ_2$	1193.39Å	-20.93%	$+1.51\%$	-1.02×10^{-1}	6.52×10^{-3}
	$3P_2 \rightarrow 3D^\circ_3$	1193.24Å	-18.74%	$+0\%$	-9.01×10^{-2}	0
S III**	$3P_2 \rightarrow 3D^\circ_1$	1202.12Å	-24.20%	$+0.95\%$	-1.20×10^{-1}	4.10×10^{-3}
	$3P_2 \rightarrow 3D^\circ_2$	1201.73Å	-20.62%	$+1.37\%$	-1.00×10^{-1}	5.90×10^{-3}
	$3P_2 \rightarrow 3D^\circ_3$	1200.97Å	-18.53%	$+0\%$	-8.90×10^{-2}	0

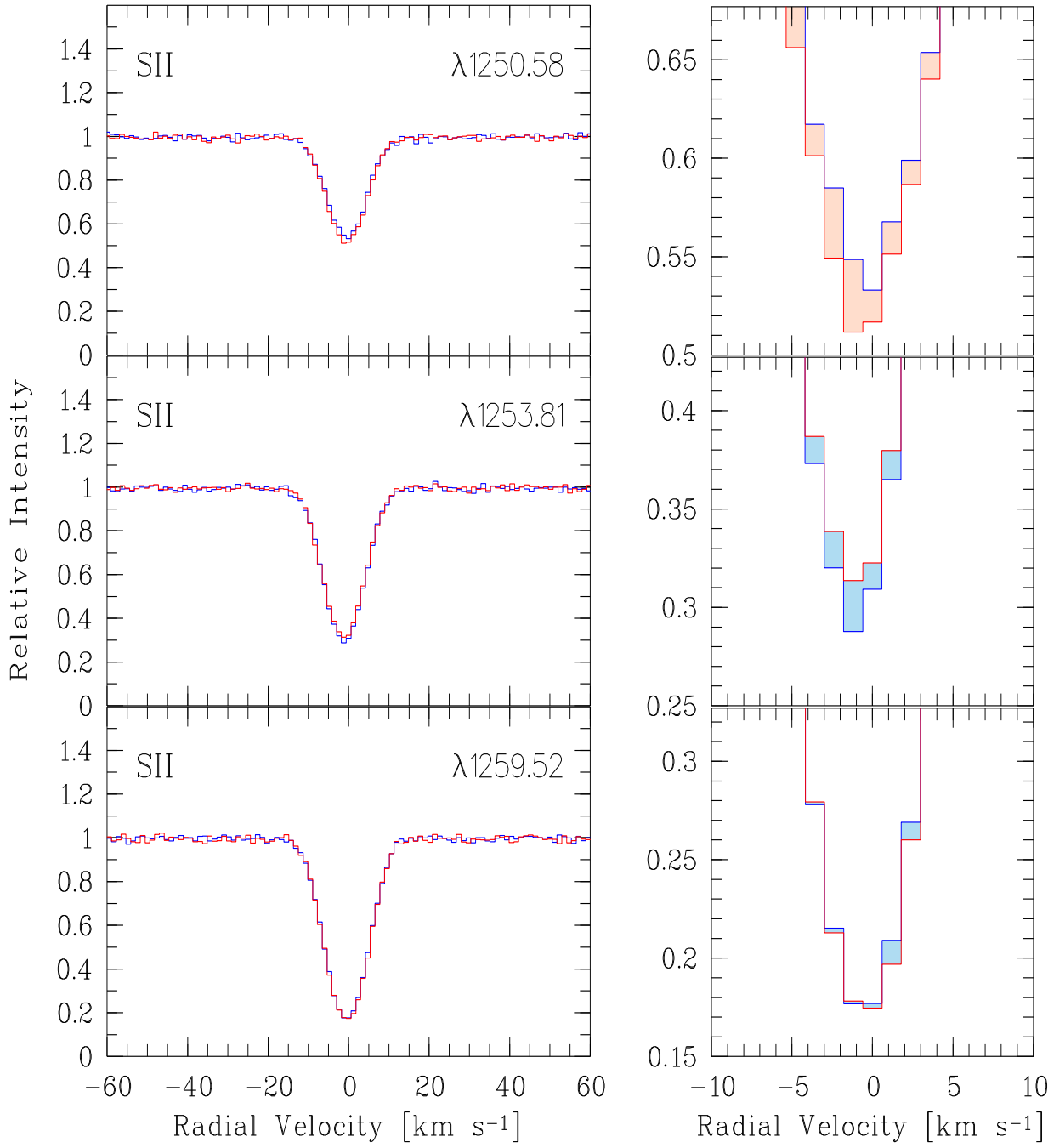

Figure 3. Synthetic spectrum (in velocity scale) of a single-component S II λλ1250.58, 1253.81, 1259.52 absorption system with a S II column density of $N(\mathrm{S\,II}) = 4 \times 10^{14}$ cm^{-2}, a Doppler paramter of $b = 5$ km s^{-1}, a spectral resolution of $R = 45,000$, and a S/N of 100 per resolution element. Such a S II column density would be expected for a DLA with log $N(\mathrm{H\,I}) = 20.48$ and a sulfur abundance of 0.1 solar assuming solar referene abundances of Asplund et al. (2009). The synthetic spectra were generated using the `FITLYMAN` routine (Fontana & Ballester 1995) implemented in the ESO-MIDAS sofware package. Atomic data were taken from Morton (2003). The blue solid line shows the orginal specrum without the atomic alignment, the red solid lines shows the spectrum including the alignment effect, assuming $\theta_0 = \theta = 90^\circ$, $\phi = 0$. The red-/blue-shaded areas indicate the excess/deficiency of absorption due to the alignment effect.

3.2.2. *Influence on emission lines*

Different from the case of absorption lines, atomic alignment for emission lines is a scattering process. The magnetic realignment on upper levels can be neglected when the precession rate of magnetic fields is smaller than the rate of emission from upper level. The alignment on the ground level can be transferred by optical excitation to upper levels, which then radiate spontaneous emission. Thus the observation of emission lines from these excited states is also influenced by the atomic alignment (see details

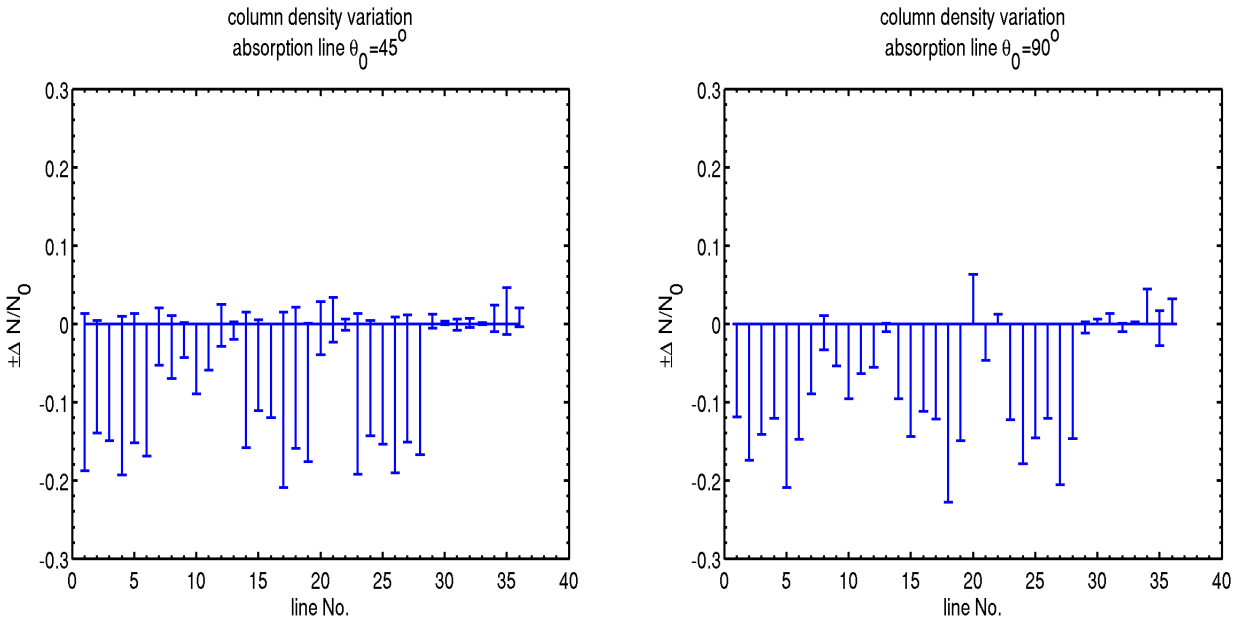

(a) (b)

Figure 4. Examples on influence of atomic alignment on column density from absorption lines. Maximum and minimum column density variations deduced from absorption lines in black-body radiation with $T_{source} = 50000K$ for (a) $\theta_0 = 45^o$ and (b) $\theta_0 = 90^o$ are presented, respectively. Value above 0 means enrichment while below means depletion. Atoms are listed in the order of element number. The line numbers on $x-axis$ represent: $1 \sim 6$, C I $\lambda\lambda$1260.93, 1261.00, 1261.12, 1193.65, 1193.39, 1193.24Å; $7 \sim 9$, C II $\lambda\lambda$1037.02, 1335.66, 1335.71Å; $10 \sim 11$, O I $\lambda\lambda$1025.76, 1027.43Å; $12 \sim 13$, Si II $\lambda\lambda$1264.74, 1265.00Å; $14 \sim 19$, S I $\lambda\lambda$1303.11, 1302.86, 1302.34, 1474.57, 1474.37, 1473.99Å; $20 \sim 22$, S II $\lambda\lambda$1250.58, 1253.81, 1259.52Å; $23 \sim 28$, S III $\lambda\lambda$1015.50, 1015.57, 1015.78, 1202.12, 1201.73, 1200.97Å; $29 \sim 30$, S IV $\lambda\lambda$1072.97, 1073.52Å;,$31 \sim 33$, Ti II $\lambda\lambda$3072.97, 3241.98, 3229.19Å; $34 \sim 36$, Fe II $\lambda\lambda$1142.36, 1143.22, 1144.923Å, respectively.

in Yan & Lazarian 2007). Given $i = 0$ in Eq. 4, the intensity of the emission lines can be expressed by:

$$I_{em}(\nu,\Omega) = \frac{h\nu_0}{4\pi} An(J_u,\theta_{br})\Psi(\nu-\nu_0)\sum_{KQ}\omega^K_{J_uJ_l}\sigma^K_Q(J_u,\theta_{br})\mathcal{J}^K_Q(0,\Omega). \tag{6}$$

Let's denote the real intensity of emission line as I^{em}_{re}; and the observed intensity of emission line as I^{em}_{ob}. The ratio between observed line intensity and real line intensity for emission lines is defined by

$$r^{em}(\lambda,\theta_0,\theta_{br},\theta) = I_{ob}/I_{re} \propto \left(\rho^0_0(J_u)\sqrt{2} + \sum_Q \omega^2_{J_uJ_l}\rho^2_Q(J_u)\mathcal{J}^K_Q(0,\Omega)\right), \tag{7}$$

where λ is the wavelength of the line, $\theta_0, \theta_{br}, \theta$ are defined in Fig. 1(a), $Q = 0, \pm1, \pm2$.

Fe II emission lines are presented as an example. The ground state of Fe II has 5 sublevels $a6D_{\frac{1}{2};\frac{3}{2};\frac{5}{2};\frac{7}{2};\frac{9}{2}}$, in which the ground level is $a6D_{J_l=\frac{9}{2}}$. The upper states of Fe II are $y6F^o_{\frac{1}{2};\frac{3}{2};\frac{5}{2};\frac{7}{2};\frac{9}{2};\frac{11}{2}}$, $z6D^o_{\frac{1}{2};\frac{3}{2};\frac{5}{2};\frac{7}{2};\frac{9}{2}}$, $z6F^o_{\frac{1}{2};\frac{3}{2};\frac{5}{2};\frac{7}{2};\frac{9}{2};\frac{11}{2}}$, $z6P^o_{\frac{3}{2};\frac{5}{2};\frac{7}{2}}$, $6D^o_{\frac{3}{2};\frac{5}{2};\frac{7}{2};\frac{9}{2}}$, etc. Two coordinate systems based on line of sight and radiation as $z-$axis respectively are compared in Fig. 6. The corresponding Fe II emission line variations with the wavelength $\lambda\lambda$1142.36, 1143.22, 1144.93 when $\theta_0 = 90^\circ$ radiation source temperature $T_{source} = 50000K$ are compared in Fig. 6(a), Fig. 6(b), and Fig. 6(c). These lines are from the excited state $y6F^o$ with different sublevels $y6F^o_{\frac{7}{2};\frac{9}{2};\frac{11}{2}}$ to the ground state $a6D_{\frac{9}{2}}$. It is obvious that with the same direction of incidental radiation and line of sight, the influence of the magnetic fields on different emission spectra is different: when $\theta = 15^\circ$, $\phi = 120^\circ$, GSA enriches λ1142.36 by 1%, enriches λ1143.22 by 8% and depletes λ1144.93 by 2%.

Moreover, even for the same spectrum with the same radiation field observed from the same line of sight (hereby, the same θ_0), the line intensity observed can be different only due to the change of magnetic fields. For example, as demonstrated in Fig. 6(b), the magnetic field almost does not influence the spectrum $\theta = 120^\circ, \phi = 120^\circ$, whereas enriches more than 10% of the spectrum when the direction of the magnetic field is perpendicular to both the line of sight and incident radiation ($\theta = 90^\circ, \phi = 90^\circ$). Therefore,taking into consideration of GSA makes the spectrum observed vary with respect to different direction of magnetic field.

Fig. 7(a) and Fig. 7(b) provide an overview on the maximum and minimum intensity variations of different emission lines

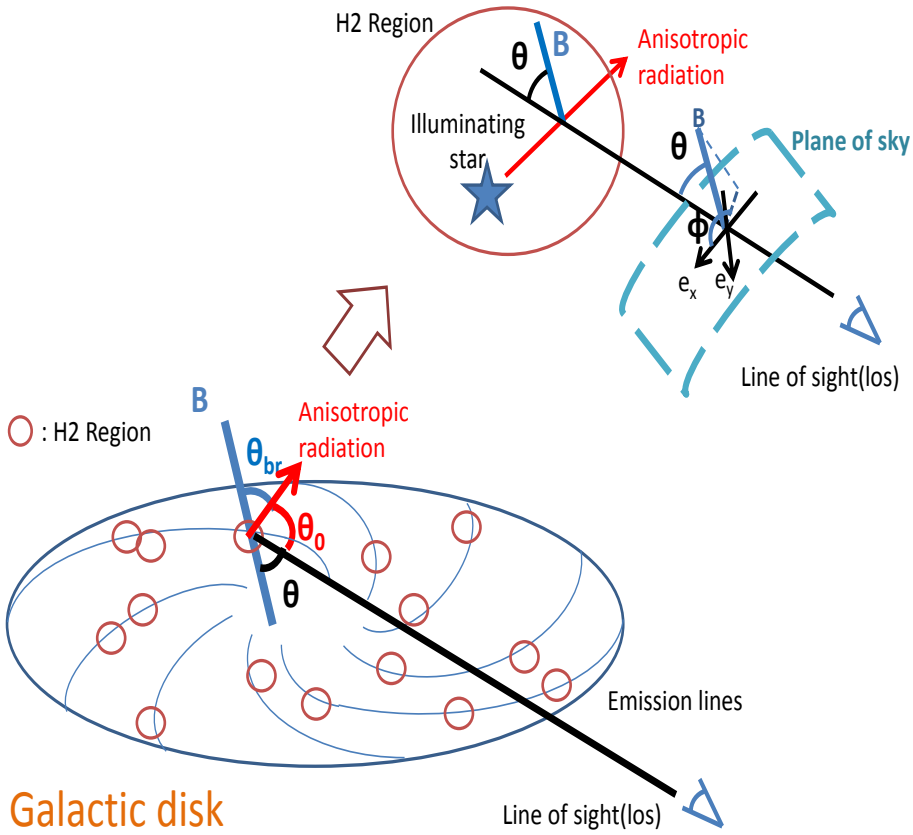

Figure 5. Scenario for atomic alignment for emission lines in extragalactic H II region. Lower plot is a spiral galaxy with H II regions denoted in red circles. It is a typical environment where emission spectra are affected by GSA. Alignment is produced by a pumping source, which provide anisotropic radiation field. θ_{br}, θ are the polar angles of the pumping radiation and line of sight measured in reference to the magnetic field, respectively. θ_0 is the angle between the anisotropic radiation and the line of sight. The upper plot depicts the influence of alignment on the scattering emission lines from H II region in detail. Stars illuminate surrounding medium which gives emission lines. The whole process is influenced by the anisotropic radiation and magnetic field due to GSA.

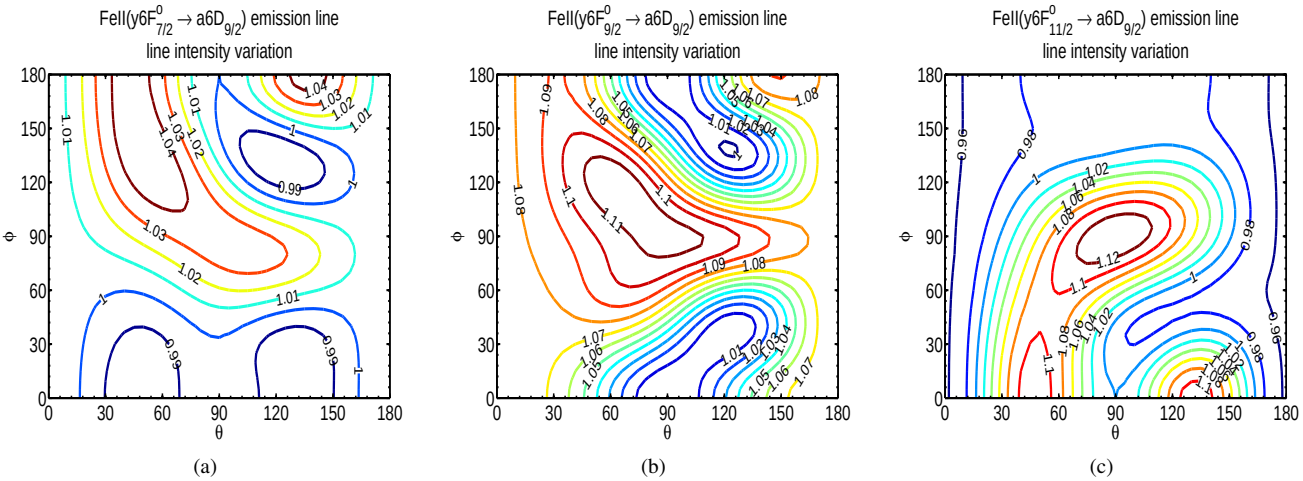

Figure 6. Fe II emission line in blackbody radiation with $T_{source} = 50000K$. Different contour represents the wavelength (a)1142.36Å; (b)1143.22Å; (c)1144.93Å in the case of line of sight vertical to radiation field($\theta_0 = 90°$).

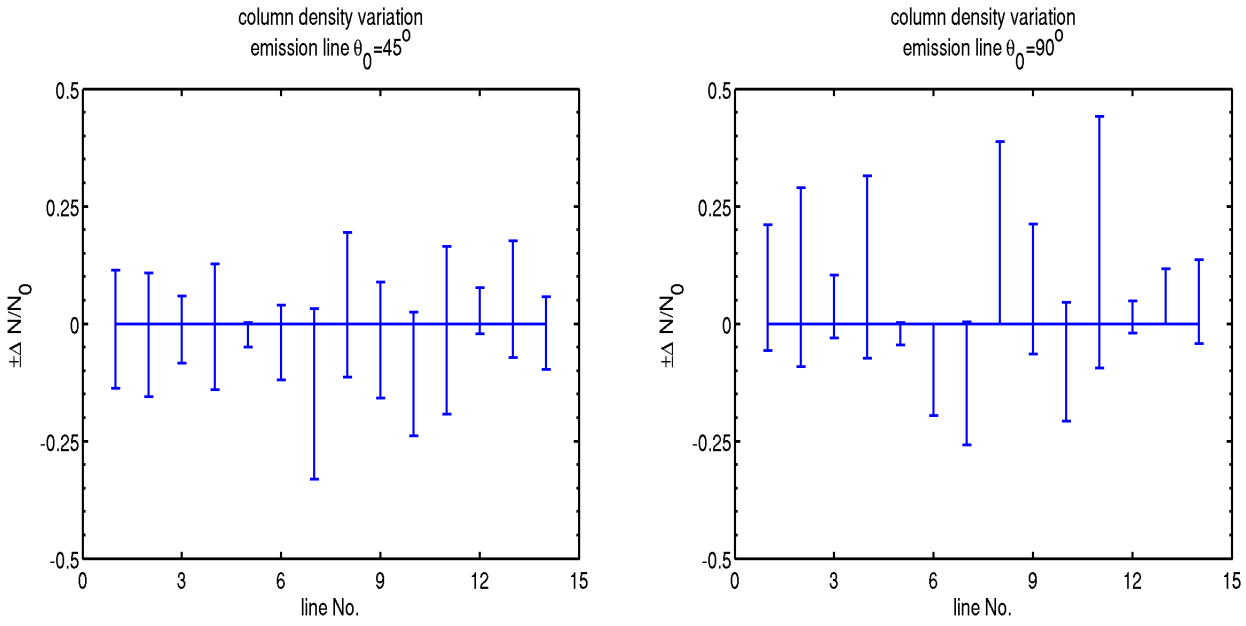

Figure 7. Examples on influence of atomic alignment on column density from emission spectra. Maximum and minimum column density variations deduced from emission lines in black-body radiation with $T_{source} = 50000K$ for (a) $\theta_0 = 45^o$ and (b) $\theta_0 = 90^o$ are presented, respectively. Value above 0 means enrichment while below means depletion. Atoms are listed in the order of element number. Only transitions that have higher probability (hereby, to the ground state mostly) are considered. The line numbers on $x-$axis represent: 1, C I λ1656.93Å; 2, C II λ1334.53Å; 3, O I λ1025.76Å; 4, Si II λ1190.42Å; $5 \sim 7$, S I λλ1474.57, 1474.37, 1473.99Å; $8 \sim 9$, S II λλ1253.81, 1259.52Å; 10, S III λ1012.49Å; 11, S IV λ1062.66Å; $12 \sim 14$, Fe II λλ1142.36, 1143.22, 1144.93Å, respectively.

with (a) $\theta_0 = 45^o$ and (b) $\theta_0 = 90^o$, respectively. The more comprehensive results for maximum and minimum variations of intensity for defferent lines are presented in Table 2, where $\Delta I/I_{max}$ means enrichment and $\Delta I/I_{min}$ means depletion. Variations on log-scale are also presented. For $\theta_0 = 90^o$, S II λ1259.52 can be depleted to the maximum of more than 6% whereas the same line can be enriched to the maximum of 22%; S I λλ1473.99 can be depleted to the maximum of more than 25% whereas the line II λ1253.81 can be enriched to the maximum of 38% , as demonstrated in Fig. 7(b). Thus it is clear that magnetic fields have different influences on different spectral lines, as well as on the same spectral line with different direction of magnetic field.

3.3. *Magnetic influence on submillimeter fine structure lines*

Submillimeter fine structure spectra, which arise from magnetic dipole transitions, have a broad applicability in astrophysics. Submillimeter lines can be used to decide chemical properties of distant star-forming galaxies and derive electron and ionization temperature of galaxy (Kobulnicky et al. 1999). They can be applied to predicting star burst size (Díaz-Santos et al. 2013). They also help the modelling of flaring Herbig Ae/Be disks (Maaskant et al. 2013).

However, previous studies do not consider atomic alignment, which in two aspects influences the results. First, in real circumstances, the assumption that radiation field is isotropic is problematic. For example, in protoplanetary disks, dominant radiation source could be localized (see Appendix A in Kama et al. 2016 for details). Moreover, the magnetic realignment has to be taken into consideration. Thus, as discussed in §2, emission and absorption coefficients for Stokes parameters will be modified due to atomic alignment.

For example, the influence of atomic alignment on C I λ610μm and Si II λ34.8μm lines are presented in Fig. 8. The ground state of C I has 3 sublevels $3P_{0;1;2}$, in which the ground level is $3P_{J_l=0}$. C I λ610μm line represents the transition within lower sublevels $3P_{J_l=1}$ and $3P_{J_l=0}$. The ground state of Si II has 2 sublevels $2P^o_{\frac{1}{2},\frac{3}{2}}$, in which the ground level is $2P^o_{J_l=\frac{1}{2}}$. Si II λ34.8μm line represents the transition within lower sublevels $2P^o_{J_l=\frac{3}{2}}$ and $2P^o_{J_l=\frac{1}{2}}$. As demonstrated in Fig. 8(a), atomic alignment can enrich C I λ610μm by 20% when $\theta = 45°, \phi = 0°$, while deplete the same line by 5% when $\theta = 120°, \phi = 45°$. In addition, by the comparison between Fig. 8(a) and Fig. 8(b), atomic alignment can enrich C I λ610μm line by a factor of more than 20% and enrich Si II λ34.8μm line by a factor of around 2% when $\theta = 45°, \phi = 45°$. Thus, atomic alignment not only has an influence on submillimeter lines obtained, but also influences different lines differently.

Fig. 9(a) and Fig. 9(b) provide an overview on the maximum and minimum column density variations from different submil-

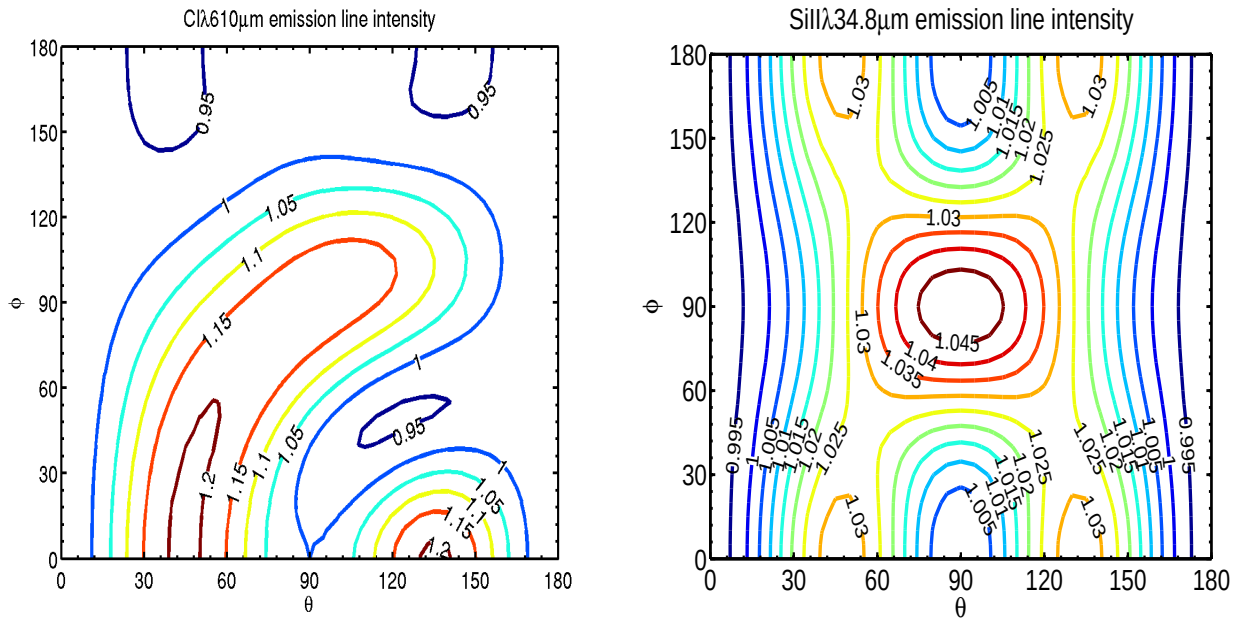

Figure 8. The variation of line intensity for submillimeter lines with respect to the direction of the magnetic field with $T_{source} = 50000K$. Contours represent the line intensity variation of (a) C I λ610μm and (b) Si II λ34.8μm with the change of magnetic field due to GSA when $\theta_0 = 90°$.

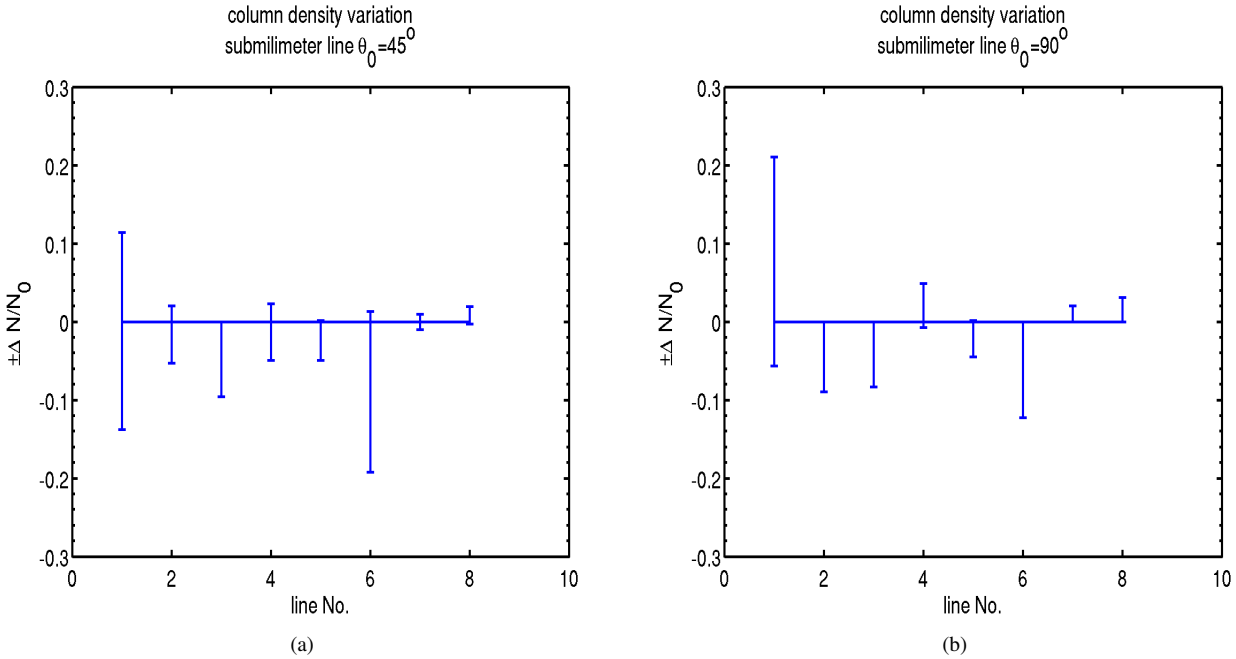

Figure 9. Examples on influence of atomic alignment on column density from submillimeter lines. Maximum and minimum column density variations deduced from submillimeter lines in blackbody radiation with $T_{source} = 50000K$ for (a) $\theta_0 = 45^o$ and (b) $\theta_0 = 90^o$ are presented, respectively. Value above 0 means enrichment while below means depletion. Atoms are listed in the order of element number. Only transitions to the ground level are considered. The line numbers on $x-$axis represent: 1, C I λ610μm; 2, C II λ157.7μm; 3, O I λ63.2μm; 4, Si II λ34.8μm; 5, S I λ25.2μm; 6, S III λ33.5μm; 7, S IV λ10.5μm; 8, Fe II λ26.0μm, respectively.

limeter lines with (a) $\theta_0 = 45^o$ and (b) $\theta_0 = 90^o$, respectively. Table 3 is provided to present the influence of atomic alignment on different submillimeter lines, where $\Delta I/I_{max}$ means enrichment and $\Delta I/I_{min}$ means depletion. It's clear that magnetic fields have different influences on different spectral lines, as well as on the same spectral line with different direction of magnetic field. For example, for $\theta_0 = 45^o$, S III $\lambda 33.5\mu m$ can be enriched to the maximum of more than 2% whereas the same line can be depleted to the maximum of almost 20% only because of the different direction of the magnetic field; C I $\lambda 610\mu m$ can be enriched to the maximum of more than 11% whereas O I $\lambda 63.2\mu m$ can be depleted to the maximum of almost 10%, as illustrated in Fig. 9(a).

4. INFLUENCE OF GSA ON PHYSICAL PARAMETERS DERIVED FROM LINE RATIO

Many important physical parameters in astronomy are derived from spectral line ratio. For example, the ratio of different transitions of C II ($\lambda 1036.34$ and $\lambda 1334.53$) is used to estimate the electron density in different astrophysical environments (see Lehner et al. 2004; Zech et al. 2008; Richter et al. 2013 for details). According to Eq. (5), the ratio of line intensity between two different lines observed from one direction for absorption line is defined by

$$\begin{aligned} \mathcal{R}^{ab}_{\lambda_1,\lambda_2}(\theta_0,\theta_{br},\theta) &= r^{ab}(\lambda_1,\theta_0,\theta_{br},\theta)/r^{ab}(\lambda_2,\theta_0,\theta_{br},\theta), \\ &\propto \frac{\rho^0_0(J'_l)\sqrt{2}+\omega^2_{J'_lJ'_u}\rho^2_0(J'_l)\left(1-1.5\sin^2\theta'\right)}{\rho^0_0(J_l)\sqrt{2}+\omega^2_{J_lJ_u}\rho^2_0(J_l)\left(1-1.5\sin^2\theta\right)}. \end{aligned} \tag{8}$$

In addition, the ratio of line intensity of emission line between two different lines observed from one direction can be obtained

Table 2. LINE INTENSITY VARIATIONS FOR EMISSION LINE INDUCED BY GSA

Species	Transition	Wavelength	$\Delta I/I_{min}$	$\Delta I/I_{max}$	$\Delta\log(N/N_0)_{min}$	$\Delta\log(N/N_0)_{max}$
C I	$3D^\circ_1 \rightarrow 3P_0$	1193.03Å	−20.85%	+21.00%	-1.02×10^{-1}	8.28×10^{-2}
C II	$2S_{\frac{3}{2}} \rightarrow 2P^\circ_{\frac{1}{2}}$	1334.53Å	−29.17%	+28.90%	-1.50×10^{-1}	1.1×10^{-1}
O I	$3D^\circ \rightarrow 3P_2$	1025.76Å	−14.30%	+10.44%	-6.70×10^{-2}	4.31×10^{-2}
Si II	$2P_{\frac{3}{2}} \rightarrow 2P^\circ_{\frac{1}{2}}$	1190.42Å	−27.20%	+31.49%	-1.38×10^{-1}	1.19×10^{-1}
S I	$3D^\circ_1 \rightarrow 3P_2$	1474.57Å	−6.32%	+0.50%	-2.84×10^{-2}	2.17×10^{-3}
	$3D^\circ_2 \rightarrow 3P_2$	1474.38Å	−19.62%	+7.49%	-9.49×10^{-2}	3.13×10^{-2}
	$3D^\circ_3 \rightarrow 3P_2$	1473.99Å	−38.67%	+3.89%	-2.12×10^{-1}	1.66×10^{-2}
S II	$4P_{\frac{3}{2}} \rightarrow 4S^\circ_{\frac{3}{2}}$	1253.81Å	−20.51%	+38.79%	-9.97×10^{-2}	1.42×10^{-1}
	$4P_{\frac{5}{2}} \rightarrow 4S^\circ_{\frac{3}{2}}$	1259.52Å	−23.04%	+21.27%	-1.14×10^{-1}	8.38×10^{-2}
S III	$3P^\circ_1 \rightarrow 3P_0$	1012.50Å	−32.02%	+6.01%	-1.68×10^{-1}	2.54×10^{-2}
S IV	$2D_{\frac{3}{2}} \rightarrow 2P^\circ_{\frac{1}{2}}$	1062.66Å	−35.44%	+44.09%	-1.90×10^{-1}	1.59×10^{-1}
Fe II	$y6F^\circ_{\frac{7}{2}} \rightarrow a6D_{\frac{9}{2}}$	1142.36Å	−2.90%	+12.10%	-1.28×10^{-2}	4.96×10^{-2}
	$y6F^\circ_{\frac{9}{2}} \rightarrow a6D_{\frac{9}{2}}$	1143.22Å	−9.37%	+22.44%	-4.27×10^{-2}	8.79×10^{-2}
	$y6F^\circ_{\frac{11}{2}} \rightarrow a6D_{\frac{9}{2}}$	1144.93Å	−14.38%	+13.64%	-6.74×10^{-2}	5.55×10^{-2}

Table 3. LINE INTENSITY VARIATIONS FOR submillimeter LINE INDUCED BY GSA

Species	Transition	Wavelength	$\Delta I/I_{min}$	$\Delta I/I_{max}$	$\Delta\log(N/N_0)_{min}$	$\Delta\log(N/N_0)_{max}$
[C I]	$3P_1 \rightarrow 3P_0$	$610\mu m$	−20.85%	+22.00%	1.02×10^{-1}	8.28×10^{-2}
[C II]	$2P^\circ_{3/2} \rightarrow 2P^\circ_{1/2}$	$157.7\mu m$	−9.02%	+3.68%	4.10×10^{-2}	1.57×10^{-2}
[O I]	$3P_1 \rightarrow 3P_2$	$63.2\mu m$	−10.77%	+0%	4.95×10^{-2}	0
[Si II]	$2P^\circ_{3/2} \rightarrow 2P^\circ_{1/2}$	$34.8\mu m$	−8.76%	+4.90%	3.98×10^{-2}	2.08×10^{-2}
[S I]	$3P_1 \rightarrow 3P_2$	$25.2\mu m$	−6.32%	+4.90%	2.84×10^{-2}	2.2×10^{-3}
[S III]	$3P^\circ_1 \rightarrow 3P_0$	$33.5\mu m$	−24.67%	+1.53%	1.23×10^{-1}	6.58×10^{-3}
[S IV]	$2P^\circ_{3/2} \rightarrow 2P^\circ_{1/2}$	$10.5\mu m$	−2.04%	+2.00%	8.96×10^{-3}	8.59×10^{-3}
[Fe II]	$a6D_{7/2} \rightarrow a6D_{9/2}$	$26.0\mu m$	−0.39%	+3.11%	1.71×10^{-3}	1.33×10^{-2}

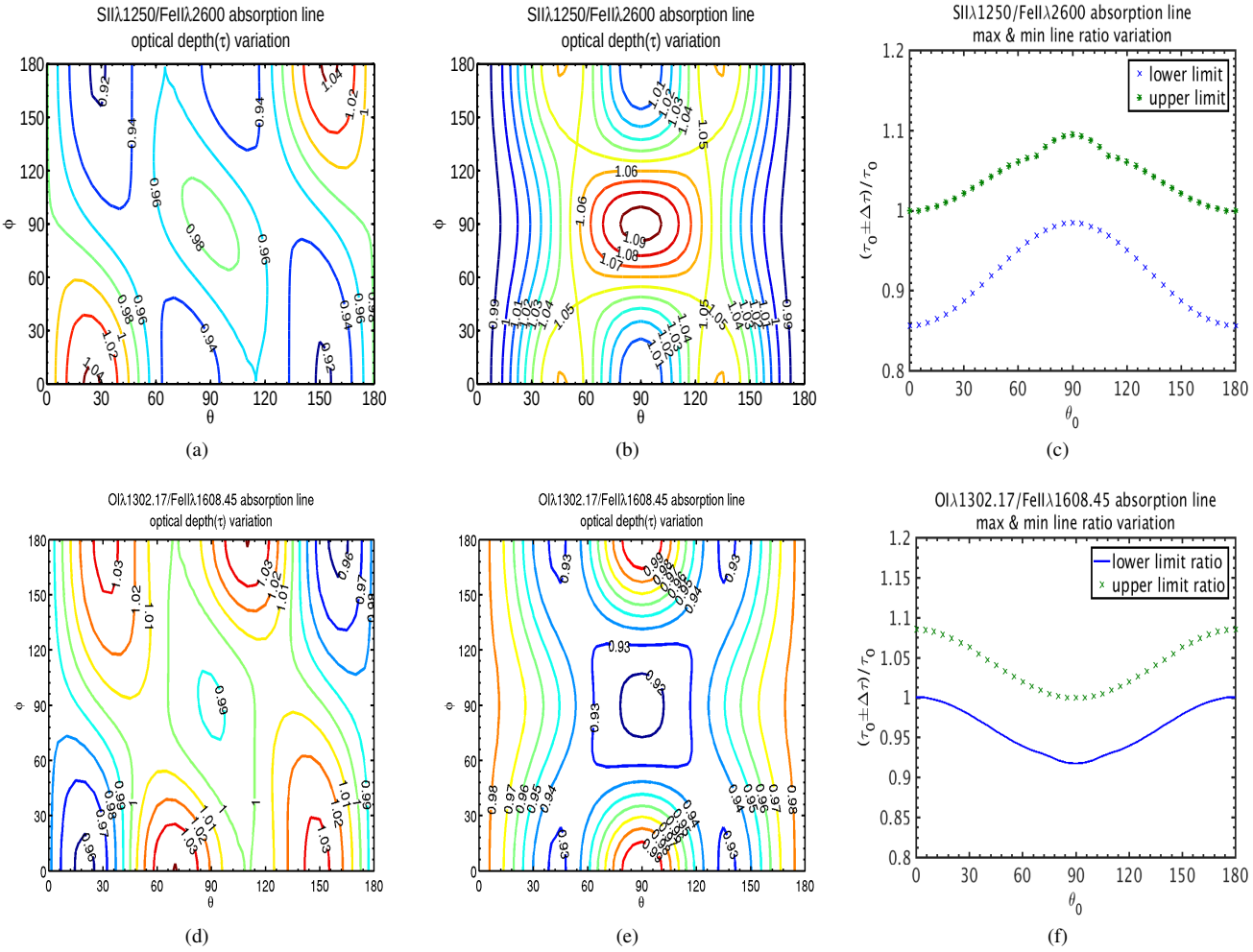

Figure 10. [α/Fe] ratio using S II λ1250/Fe II λ2599 and O I λ1302.17/ Fe II λ1608.45 absorption line ratios in blackbody radiation with $T_{source} = 50000K$. Line ratio with the case when the magnetic field is parallel to the direction of incidental radiation is set as 1. (a),(b) The variation of line ratio S II λ1250/Fe II λ2599 with respect to the direction of the magnetic field when $\theta_0 = 45°$ and $\theta_0 = 90°$ respectively; (c) The maximum and minimum ratio S II λ1250/Fe II λ2599 with respect to different θ_0; (e),(f) The variation of line ratio O I λ1302.17/ Fe II λ1608.45 with respect to the direction of the magnetic field in the case when $\theta_0 = 45°$ and $\theta_0 = 90°$ respectively; (g) The maximum and minimum ratio O I λ1302.17/ Fe II λ1608.45 with respect to different θ_0.

from Eq. (7):

$$\mathcal{R}^{em}_{\lambda_1,\lambda_2}(\theta_0,\theta_{br},\theta) = r^{em}(\lambda_1,\theta_0,\theta_{br},\theta)/r^{em}(\lambda_2,\theta_0,\theta_{br},\theta),$$
$$\propto \frac{\left(\rho^0_0(J'_u)\sqrt{2}+\sum_Q \omega^2_{J'_uJ'_l}\rho^2_Q(J'_u)\mathcal{J}^K_Q(0,\Omega)\right)}{\left(\rho^0_0(J_u)\sqrt{2}+\sum_Q \omega^2_{J_uJ_l}\rho^2_Q(J_u)\mathcal{J}^K_Q(0,\Omega)\right)}. \tag{9}$$

Since the depletion and enrichment of different spectral lines vary with the same magnetic field, the influence on spectral line ratio can be expected to be more significant with one line depleted and the other enriched. A few examples will be presented in the following subsections.

4.1. *Influence on nucleosynthetic studies in DLAs*

The alpha-to-iron ratio is widely used in spectral analysis. This line ratio comparison reflects the nucleosynthetic processes in star forming region (e.g., Prochaska et al. 2001; Prochaska & Wolfe 2002). The α elements can be measured by elements like O, Si, S, Ti etc, whereas Fe refers to Fe peak elements like Cr, Mn, Co, Fe etc. α elements like O and Fe in the medium of the galaxy with low metallicity ([Fe/H]$\lesssim$-1.0) are produced exclusively by Type-II supernovae(SNe II), but the [α/Fe] ratio suffers a drop when the delayed contribution of Fe from Type-Ia supernovae (SNe Ia) is effective (McWilliam 1997; Cooke et al. 2011). The alpha-to-iron ratio [X/Fe] (X represents the chemical elements for α elements) is defined by the ratio of abundance observed

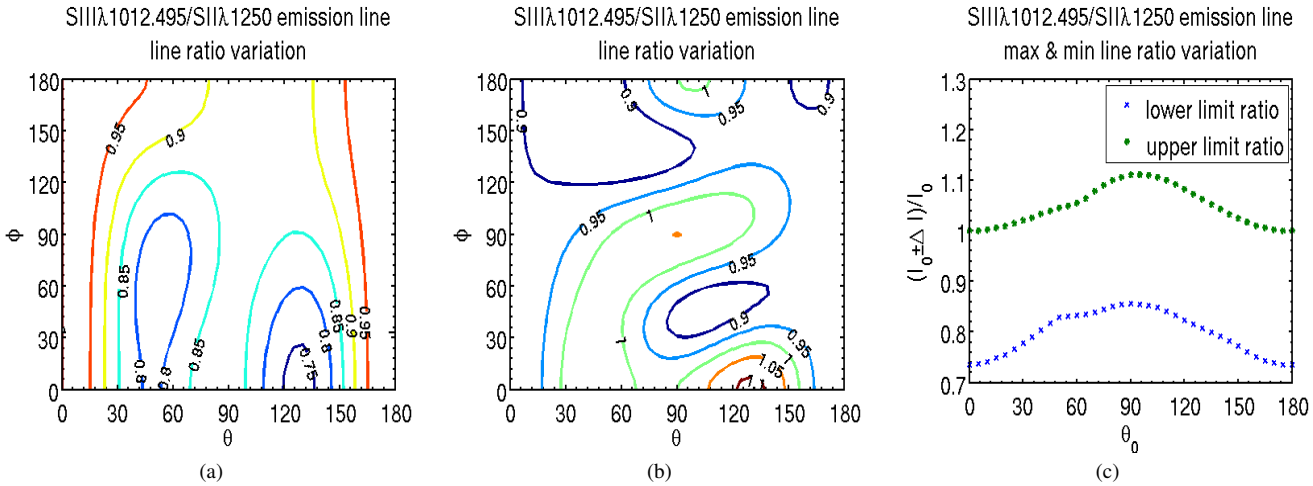

Figure 11. Line ratio of S III λ1012.49 and S II λ1250.58 absorption line in blackbody radiation with $T_{source} = 50000K$. Line ratio with the case when the magnetic field is parallel to the direction of incident radiation is set as 1. (a),(b) The variation of line ratio with respect to the direction of the magnetic field in the case of line of sight parallel and vertical to radiation field($\theta_0 = 0°, 90°$, respectively); (c) The maximum and minimum ratio with respect to different θ_0.

from the medium in comparison with that from the sun:

$$[X/Fe] \equiv log[N(X)/N(Fe)] - log[N(X)/N(Fe)]_{\odot} \tag{10}$$

The abundance of the elements is assumed to be equal to the column density of the dominant ionization state. For example, Fe II lines are used for Fe abundance and S II for S since in DLAs these elements are mostly single ionized. Thus, the ratio N(S)/N(Fe) can be obtained by measuring $\mathcal{R}^{ab}_{SII,FeII}$. When GSA is taken into consideration, the variation of the ratio S II/Fe II with respect to different direction of magnetic fields when $\theta_0 = 45°$ and $\theta_0 = 90°$ are presented in Fig. 10(a) and Fig. 10(b), respectively. As demonstrated in Fig. 10(c), the variation for N(S)/N(Fe) when taken into account of GSA is $[-14\%, +10\%]$, which makes the variation in log-scales [-0.04,+0.07]. If $\log[N(X)/N(Fe)]_{\odot}$ obtained from solar is considered to be fixed, the influence of GSA on [S/Fe] is [-0.07,+0.06].

In comparison, another α element O is presented as an example. Most O in DLAs are neutral and hence the ratio N(O)/N(Fe) can be represented by $\mathcal{R}^{ab}_{OI,FeII}$. The influence of GSA on the line ratio O Iλ1302.17/Fe IIλ1608.45 when $\theta_0 = 45°$ and $\theta_0 = 90°$ are presented in Fig. 10(d) and Fig. 10(e), respectively. By comparing Fig. 10(a) and Fig. 10(e), it is obvious that when magnetic field is parallel to both the line of sight and incidental radiation, the alignment enriches N(S)/N(Fe) by 10% whereas depletes N(O)/N(Fe) by 9%. As a result, with the same direction of magnetic field and the same line of sight, [S/Fe] observed varies $+0.06$ while [O/Fe] observed varies -0.06. Hence, GSA will affect results from nucleosynthetic studies, although the effect is small, in particular when compared to possible ionization effect.

4.2. *Influence on ionization studies in diffuse gas*

The ratio of the abundance[9] of different ionization states of the same element is often used to depict the ionization rate (see e.g., Richter et al. 2016). As an example, (S III)/(S II) emission line ratio can be applied to decide the ionization rate in extragalactic H II region (see e.g., Vilchez et al. 1988), because higher ionized Sulphur is not important in most of these H II regions (Mathis 1982, 1985). To illustrate the influence of GSA, the line ratio S III λ1012.49/S II λ1250.58 is used to represent (S III)/(S II). Fig. 11(a) and Fig. 11(b) demonstrate the influence of GSA with different direction of magnetic fields when $\theta_0 = 0°$ and 90°. As presented in Fig. 11(c), the variation under the influence of GSA is $[-27\%, +12\%]$, which means a variation of [-0.14,+0.05] on log[N(S III)/N(S II)]. Therefore, the influence of GSA on the ionization rate is ineligible.

5. DISCUSSIONS

GSA is a well-studied effect in laboratory, whilst its importance still requires attention in astrophysical community. In this paper, we generate synthetic spectra according to a scenario about DLAs in galaxy to present the change of observed spectrum with the influence of magnetic fields under the influence of GSA. We demonstrate the variation of emission lines due to GSA in a scenario of extragalactic H II Region. The influence of GSA on submillimeter fine-structure lines is discussed under a scenario

[9] The abundance ratio can be analyzed from both absorption ratios and emission ratios.

for star forming regions. The variations that GSA causes to physical parameters derived from spectral line ratios are analysed. Real observational data may be used to compare with the theoretical predictions to trace the effect. Nevertheless, the effect is not limited to the examples that we provide. Meanwhile, some physical processes that may influence the alignment can be taken into account in further studies. We present some future outlooks as follows:

5.1. *Observation of the effect and Hyperfine splitting*

As illustrated in this paper, GSA has a small but measurable influence in spectroscopic observation. Thus, if several transitions from the same species (atom/ion) are available in a given line spectrum, the GSA effect can be measured from the *differential* changes in the line intensity of these lines in future work, because the individual lines are affected *differently*. However, since in some cases the effect is expected to be small (see §3), an experiment on the effect for certain elements may require a high spectral resolution and a high signal-to-noise (S/N) ratio. Furthermore, as illustrated in (Yan & Lazarian 2007), hyperfine splitting of atoms and ions will also influence the alignment. Even with the same fine structure, the atoms with hyperfine structure (the nuclear spin is not 0) is affected by GSA differently than the atoms without (see the comparison between the alignment of S II and N I in Fig. 19 in Yan & Lazarian 2007, in which the two elements share the same atomic fine structure, but due to a different nuclear spin, the alignment on the ground state of the two elements are totally different). The alignment on different hyperfine sublevels of the same fine structure level can be different. Hence, future observations with higher resolution that can separate transitions to different hyperfine sublevels will be perfect for analyzing the influence of magnetic fields because the span of the hyperfine lines are so small that they would share the same signal-to-noise(S/N) ratio. Note that hyperfine splitting also has to be considered when studying the GSA effect on fine structure transitions of the atoms with nuclear spin.

5.2. *fluorescence lines*

As illustrated in §3.2, the alignment on the ground state can be transferred to the upper state through absorption process. Atoms in upper states quickly decay by radiative transitions and hence photons are emitted. In real circumstances, the excited atoms may experience several decays and photons emitted may be scattered several times before they actually escape, which can be considered in future work. The intensity of the lines derived from successive decays to different levels of atoms are thus dependent on the density of the initial upper levels, which can be influenced by GSA by scattering process demonstrated in Fig. 5.

5.3. *The influence of strong magnetic fields*

In most interstellar medium where the magnetic field is relatively weak (1 Gauss$\gtrsim$ B $\gtrsim 10^{-15}$ Gauss), the GSA is applicable for the influence of magnetic field on spectral lines. However the influence of magnetic fields on photon-excited spectra is not limited to this range. Stronger magnetic fields (B > 1 Gauss) can also affect the spectra observed (e.g., spectra from stars) due to the upper level Hanle effect (see Landi Degl'Innocenti & Landolfi 2004).

5.4. *The influence of collision*

The influence of collision is negligible in this paper, which applies to most diffuse interstellar medium. However, collision can become important in the case of higher density and higher temperature medium. The threshold for collision being more important than optical pumping is when the collision rate τ_C^{-1}(either inelastic collision rate or Van der Waals collision rate) is larger than optical pumping rate $B_{J_l J_u} I$ (see Yan & Lazarian 2006 for details). Collisions can also redistribute atoms to different sublevels, yet a reduced efficiency is expected (see Hawkins 1955). In higher temperature H II Regions, collision energy may be enough to excite atoms partially to the metastable levels from the ground level. Hence, the recombination lines and collisional excited lines can be combined together to evaluate the influence of GSA in future work.

6. SUMMARY

We have demonstrated the influence of magnetic fields due to GSA on spectroscopic studies. We emphasize that GSA is a general physical process that can affect both absorption and emission spectra. Examples of absorption and emission lines observed from different astrophysical environment have been presented to demonstrate the influence of GSA. Our main conclusions are:

- Due to GSA, magnetic fields will affect absorption and emission spectral lines.
- Physical parameters derived from line ratios can be influenced by GSA.
- The depletion and enrichment of the same spectrum due to GSA depends on the direction of the magnetic field.
- The influence of GSA varies with different spectral lines.

- Due to GSA, magnetic fields will affect absorption spectra from absorbers' continuum to analysis diffuse medium like DLAs and galactic halos. For current observational data, the GSA effect on certain elements may require high resolution and high signal-to-noise ratio.
- The observations for emission spectra from diffuse medium like extragalactic H II Regions, circumburst medium near GRBs, and supernova remnants can be influenced by GSA through a scattering process.
- GSA can affect submillimeter fine-structure lines from diffuse medium like PDR regions, star forming regions and Herbig Ae/Be disks, etc.
- The influence of GSA on spectral line ratio can reach more than 25% in some cases.

APPENDIX

A. BASIC FORMULAE ON ATOMIC ALIGNMENT

In this Appendix, we illustrate the basic equations on GSA and address the point in §2 on how the magnetic fields affect the density of atoms on ground level($\rho(J_l)$) and upper level($\rho(J_u)$) due to GSA.

Anisotropic radiation can excite atoms, which is known as photo-excitations and consequently results in spontaneous emissions. As is well illustrated in previous GSA papers, both the photo-excitation and magnetic precession decide the occupations among the sublevels of the ground state. The equations to describe the evolution of atom densities on both upper and ground states are (see Landi Degl'Innocenti & Landolfi 2004):

$$\dot{\rho}^k_q(J_u)+2\pi i\nu_L g_u q\rho^k_q(J_u)= -\sum_{J_l}A(J_u\rightarrow J_l)\rho^k_q(J_u)+\sum_{J_lk'}[J_l]\left[\delta_{kk'}p_{k'}(J_u,J_l)B_{lu}\bar{J}^0_0+\sum_{Qq'}r_{kk'}(J_u,J_l,Q,q')B_{lu}\bar{J}^2_Q\right]\rho^{k'}_{-q'}(J_l), \tag{A1}$$

$$\dot{\rho}^k_q(J_l)+2\pi i\nu_L g_l q\rho^k_q(J_l)= \sum_{J_u}p_k(J_u,J_l)[J_u]A(J_u\rightarrow J_l)\rho^k_q(J_u)-\sum_{J_uk'}\left[\delta_{kk'}B_{lu}\bar{J}^0_0+\sum_{Qq'}s_{kk'}(J_u,J_l,Q,q')B_{lu}\bar{J}^2_Q\right]\rho^{k'}_{-q'}(J_l), \tag{A2}$$

in which

$$p_k(J_u,J_l)=(-1)^{J_u+J_l+1}\left\{\begin{array}{ccc}J_l & J_l & k\\ J_u & J_u & 1\end{array}\right\},p_0(J_u,J_l)=\frac{1}{\sqrt{[J_u,J_l]}}, \tag{A3}$$

$$r_{kk'}(J_u,J_l,Q,q)=(3[k,k',2])^{\frac{1}{2}}\left\{\begin{array}{ccc}1 & J_u & J_l\\ 1 & J_u & J_l\\ 2 & k & k'\end{array}\right\}\left(\begin{array}{ccc}k & k' & K\\ q & q' & Q\end{array}\right), \tag{A4}$$

$$s_{kk'}(J_u,J_l,Q,q)=(-1)^{J_l-J_u+1}[J_l](3[k,k',K])^{\frac{1}{2}}\left(\begin{array}{ccc}k & k' & 2\\ q & q' & Q\end{array}\right)\left\{\begin{array}{ccc}1 & 1 & 2\\ J_l & J_l & J_u\end{array}\right\}\left\{\begin{array}{ccc}k & k' & 2\\ J_l & J_l & J_l\end{array}\right\}. \tag{A5}$$

The evolution of the ground state $[\rho^k_q(J_l)]$ and the upper state $[\rho^k_q(J_u)]$ are illustrated in Eq. (A2) and Eq. (A1), respectively. The quantities J_u and J_l are the total angular momentum quantum numbers for the upper and lower levels, respectively. The quantity A is the Einstein spontaneous emission rate and the quantity B is the Einstein coefficient for absorption and stimulated emission. The quantities ρ^k_q and $\bar{J}^K_Q$ are irreducible density matrices for the atoms and the radiation field, respectively. $6-j$ and $9-j$ symbols are represented by the matrices with "{ }", whereas $3-j$ symbols are indicated by the matrices with "()" (see Zare & Harter 1989 for details). The symbol $[j]$ represents the quantity $2j+1$, e.g., $[J_l]=2J_l+1$, $[J_l,J_u]=(2J_l+1)(2J_u+1)$, etc. *The second terms on the left side of Eq.* (A1) *and Eq.* (A2) *stand for the magnetic realignment.* Due to fast magnetic precession, magnetic realignment on the upper levels can be neglected. The two terms on the right side represent spontaneous emissions and the excitations from lower levels. All the transitions to different upper states and different sublevels of the ground state are taken into account by summing up J_u and J_l. Note that the symmetric processes of spontaneous emission and magnetic realignment

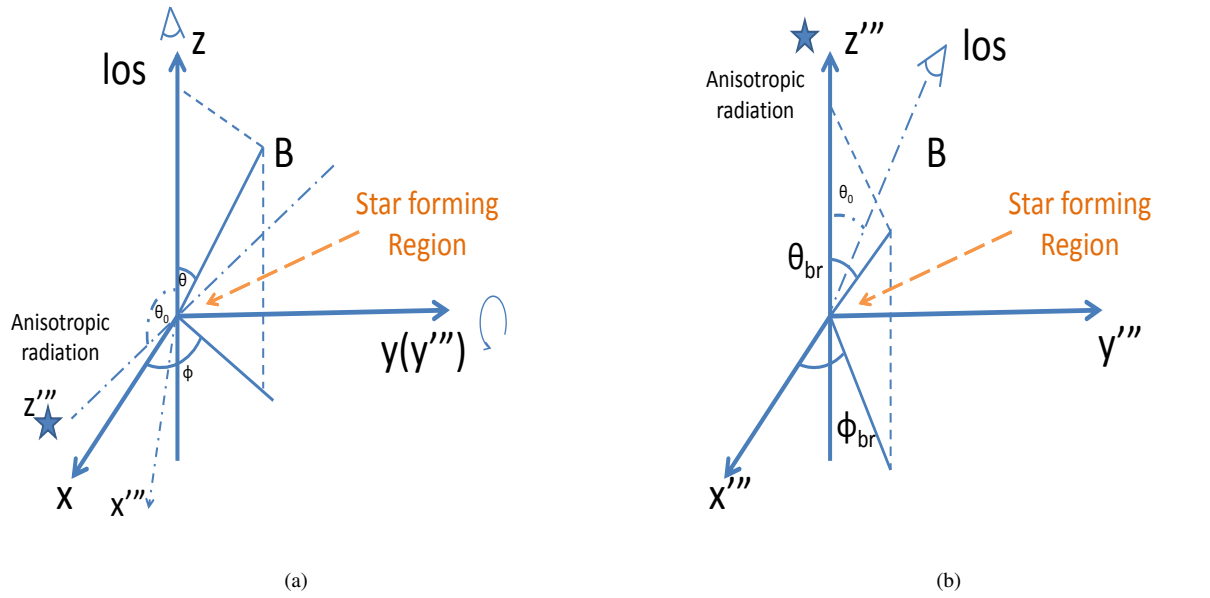

Figure B1. Different coordinate system for comparison. The variation of line intensity with respect to the direction of the magnetic field is compared to the spectrum when magnetic field is parallel to the incidental radiation. (a) $xyz-$coordinate system with line of sight being $z-$axis; θ and ϕ are the polar and azimuth angle of the magnetic field in line of sight coordinate; (b) $x'''y'''z'''-$coordinate system with radiation field being $z'''-$axis; θ_{br} and ϕ_{br} are the polar and azimuth angle of the magnetic field in radiation coordinate.

conserve k and q. Hence, the steady state occupations of atoms on the ground state are obtained by setting the left side of Eq. (A1) and Eq. (A2) zero:

$$2\pi i\rho^k_q(J_l)qg_l\nu_L - \sum_{J_uk'}\left\{p_k(J_u,J_l)\frac{[J_u]}{\sum_{J_l''}A''/A+i\Gamma' q}\sum_{J_l'}B_{lu}[J_l']\left[\delta_{kk'}p_{k'}(J_u,J_l')\bar{J}^0_0+\sum_{Qq'}r_{kk'}(J_u,J_l',Q,q')\bar{J}^2_Q\right]\right.$$
$$\left.-\delta_{J_lJ_l'}\left[\delta_{kk'}B_{lu}\bar{J}^0_0+\sum_{Qq'}B_{lu}s_{kk'}(J_u,J_l,Q,q')\bar{J}^2_Q\right]\right\}\rho^{k'}_{-q'}(J_l')=0 \tag{A6}$$

where Γ' equals $2\pi\nu_L g_u/A$. Solving the above equations, the density of atoms on different levels($\rho^k_q(J_l)$, $\rho^{k'}_{q'}(J_u)$) under the influence of magnetic fields can be obtained. Thus the alignment parameter (σ^K_Q) can be achieved by using the definition $\sigma^K_Q\equiv\frac{\rho^K_Q}{\rho^0_0}$.

B. COMPARISON OF DIFFERENT COORDINATE SYSTEM

Throughout the paper, in order to show the GSA effect with the change of magnetic fields, we fix the direction of line of sight and the direction of incidental radiation for all the contour plots. However, with this setting, two coordinate systems can be used to depict the change of magnetic fields. $xyz-$coordinate system with the line of sight as $z-$axis is presented in Fig. 1(a), which is considered as the real observation structure. The coordinate system with radiation as $z'''-$axis and the corresponding spectral variations are presented in Fig. 1(b).

As an example to compare the two coordinate systems, the influence of atomic alignment on S III $\lambda33.5\mu m$ is presented in Fig. B2. The ground state of S III has 3 sublevels $3P_{0;1;2}$, in which the ground level is $3P_{J_l=0}$. S III $\lambda33.5\mu m$ line represents the transition within lower sublevels $3P_{J_l=1}$ and $3P_{J_l=0}$. Fig. 2(a) shows the variation of the line intensity S III$\lambda33.5\mu m$ when $\theta_0=45^\circ$ in $xyz-$coordinate system in Fig. 1(a). Fig. 2(b) shows the variation of the line intensity S III$\lambda33.5\mu m$ when $\theta_0=45^\circ$ in $x'''y'''z'''-$coordinate system in Fig. 1(b). As illustrated in Eq. (A6), as the angle θ_{br} is fixed, the alignment parameter σ^2_0 is the same. As a result, in Fig. 2(b), the change of ϕ_{br} under the same θ_{br} means the spectra with the same alignment observed from different line of sight.(For example, by comparing Fig. 2(a) and Fig. 2(b), it is obvious that spectra with the same alignment (same θ_{br} in Fig. 2(b)) have a smaller variation.) Thus $x'''y'''z'''-$coordinate system exhibits a more explicit physical meaning than $xyz-$coordinate system. However, by comparing the same situation in different coordinate systems, it is obvious that the maximum and minimum variations of the two plots remain the same. For the sake of observation, we present our results through the paper with the actual observation system: $xyz-$coordinate system with the line of sight magnetic angle θ and the plane of sky magnetic angle ϕ, as well defined in the scenarios Fig. 1(a) and Fig. 5.

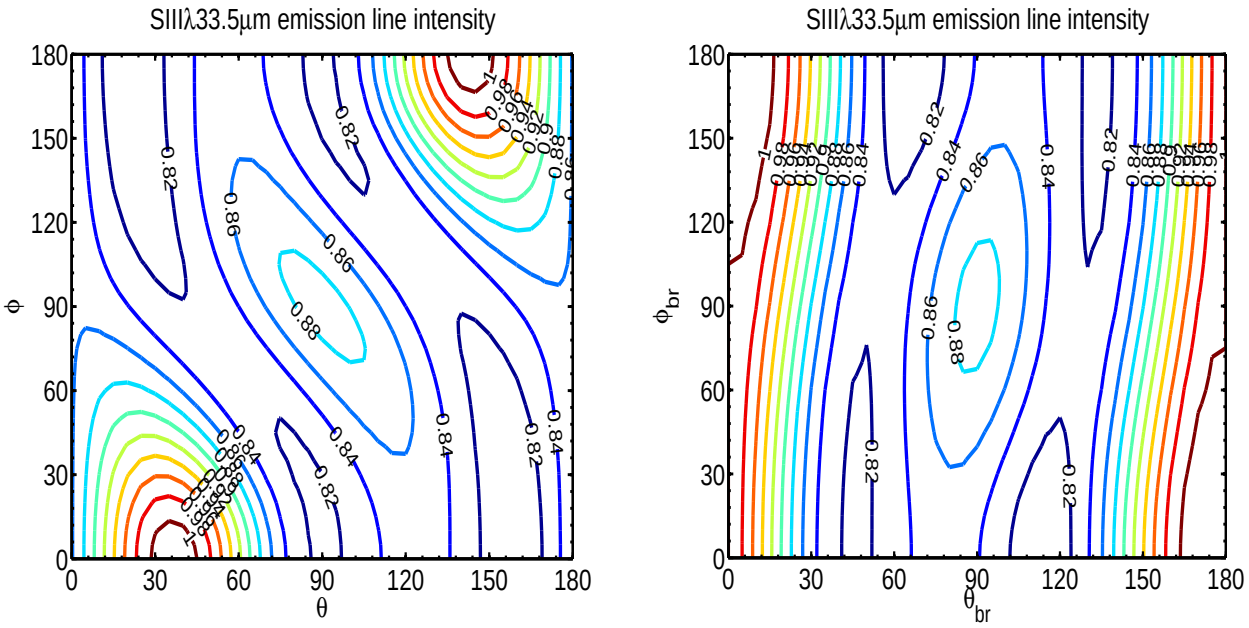

Figure B2. The variation of line intensity for submillimeter lines with respect to the direction of the magnetic field with $T_{source} = 50000K$. Contours are presented in different coordinate system defined in Fig. B1 for the line intensity variation of S III $\lambda 33.5\mu m$ when $\theta_0 = 45°$, respectively. (a) θ and ϕ are the polar and azimuth angle of the magnetic field in line of sight coordinate defined in Fig. 1(a); (b) θ_{br} and ϕ_{br} are the polar and azimuth angle of the magnetic field in line of sight coordinate defined in Fig. 1(b).

C. SUMMARY OF ANGLES USED IN THE PAPER

angle between radiation and line of sight in Fig. 1(b)	θ_0
angle between line of sight and magnetic field in Fig. 1(b)	θ
azimuth coordinates in axial frame where line of sight is $z-$axis in Fig. 1(b)	ϕ
angle between radiation direction and magnetic field in Fig. 1(b)	θ_{br}
azimuth coordinates in $xyz-$frame in Fig. 1(d)	ϕ_r
azimuth coordinates in $x'''y'''z'''-$frame in Fig. 1(b)	ϕ_{br}

REFERENCES

Asplund, M., Grevesse, N., Sauval, A. J., & Scott, P. 2009, ARA&A, 47, 481

Bruhweiler, F., & Verner, E. 2008, ApJ, 675, 83

Ceccarelli, C., Hollenbach, D. J., & Tielens, A. G. G. M. 1996, ApJ, 471, 400

Cooke, R., Pettini, M., Steidel, C. C., Rudie, G. C., & Nissen, P. E. 2011, MNRAS, 417, 1534

Díaz-Santos, T., Armus, L., Charmandaris, V., et al. 2013, ApJ, 774, 68

Esteban, C., García-Rojas, J., Carigi, L., et al. 2014, MNRAS, 443, 624

Fontana, A., & Ballester, P. 1995, The Messenger, 80, 37

Fox, A., Richter, P., & Fechner, C. 2014a, A&A, 572, A102

Fox, A. J., Richter, P., Wakker, B. P., et al. 2013, ApJ, 772, 110

Fox, A. J., Wakker, B. P., Barger, K. A., et al. 2014b, ApJ, 787, 147

Fynbo, J. P. U., Starling, R. L. C., Ledoux, C., et al. 2006, A&A, 451, L47

García-Rojas, J., Corradi, R. L. M., Monteiro, H., et al. 2016, ApJL, 824, L27

Hawkins, W. B. 1955, Physical Review, 98, 478

Howk, J. C., Wolfe, A. M., & Prochaska, J. X. 2005, ApJL, 622, L81

Jerkstrand, A., Fransson, C., & Kozma, C. 2011, A&A, 530, A45

Kama, M., Bruderer, S., Carney, M., et al. 2016, ArXiv e-prints, arXiv:1601.01449

Kastler, A. 1950, J. Phys. Radium, 11, 255

Kisielius, R., Kulkarni, V. P., Ferland, G. J., Bogdanovich, P., & Lykins, M. L. 2014, ApJ, 780, 76

Kobulnicky, H. A., Kennicutt, Jr., R. C., & Pizagno, J. L. 1999, ApJ, 514, 544

Landi Degl'Innocenti, E. 1984, SoPh, 91, 1

Landi Degl'Innocenti, E., & Landolfi, M., eds. 2004, Astrophysics and Space Science Library, Vol. 307, Polarization in Spectral Lines

Landolfi, M., & Landi Degl'Innocenti, E. 1986, A&A, 167, 200

Lehner, N., Wakker, B. P., & Savage, B. D. 2004, ApJ, 615, 767

Leitherer, C., Hernandez, S., Lee, J. C., & Oey, M. S. 2016, ApJ, 823, 64

Maaskant, K. M., Honda, M., Waters, L. B. F. M., et al. 2013, A&A, 555, A64

Mathis, J. S. 1982, ApJ, 261, 195

—. 1985, ApJ, 291, 247

McWilliam, A. 1997, ARA&A, 35, 503

Meiring, J. D., Tripp, T. M., Prochaska, J. X., et al. 2011, ApJ, 732, 35

Miller, M. J., & Bregman, J. N. 2015, ApJ, 800, 14
Morton, D. C. 2003, ApJS, 149, 205
Peimbert, M., & Peimbert, A. 2006, in IAU Symposium, Vol. 234, Planetary Nebulae in our Galaxy and Beyond, ed. M. J. Barlow & R. H. Méndez, 227–234
Pickering, J. C., Thorne, A. P., & Perez, R. 2001, ApJS, 132, 403
Prochaska, J. X., & Wolfe, A. M. 2002, ApJ, 566, 68
Prochaska, J. X., Wolfe, A. M., Tytler, D., et al. 2001, ApJS, 137, 21
Richter, P., Fox, A. J., Wakker, B. P., et al. 2013, ApJ, 772, 111
Richter, P., Sembach, K. R., Wakker, B. P., et al. 2001, ApJ, 559, 318
Richter, P., Wakker, B. P., Fechner, C., et al. 2016, A&A, 590, A68
Savage, B. D., & Sembach, K. R. 1996, ARA&A, 34, 279
Stutzki, J., Stacey, G. J., Genzel, R., et al. 1988, ApJ, 332, 379
Varshalovich, D. A. 1968, Astrofizika, 4, 519
—. 1971, Soviet Physics Uspekhi, 13, 429
Vilchez, J. M., Pagel, B. E. J., Diaz, A. I., Terlevich, E., & Edmunds, M. G. 1988, MNRAS, 235, 633
Welsh, B. Y., & Lallement, R. 2012a, PASP, 124, 566
—. 2012b, PASP, 124, 566
Yan, H., & Lazarian, A. 2006, ApJ, 653, 1292
—. 2007, ApJ, 657, 618
—. 2008, ApJ, 677, 1401
—. 2012, JQSRT, 113, 1409
—. 2013, ArXiv e-prints, arXiv:1302.3264
Zare, R. N., & Harter, W. G. 1989, Physics Today, 42, 68
Zech, W. F., Lehner, N., Howk, J. C., Van Dyke Dixon, W., & Brown, T. M. 2008, ApJ, 679, 460
Zhang, H., Yan, H., & Dong, L. 2015, ApJ, 804, 142